Dissertation submitted to the
Combined Faculties for the Natural Sciences and for Mathematics
of the Ruperto-Carola University of Heidelberg, Germany
for the degree of
Doctor of Natural Sciences

Put forward by
Diplom-Physiker: Claas Wessels
Born in: Essen
Oral examination: January 2017

Uncertainties in modern radiotherapy: Tomotherapy and RapidArc

Referees:
Prof. Dr. Uwe Oelfke
Prof. Dr. Joao Seco

Zusammenfassung

Die vorliegende Arbeit konzentriert sich auf Unsicherheiten, die entlang des Verlaufs der externen Strahlentherapie auftreten.
Zunächst wurde getestet und beurteilt, ob die Qualität der Detektoren, die verwendet werden, um Unsicherheiten und deren Gründe zu analysieren und um zu entscheiden, ob ein Plan akzeptabel ist oder nicht, ausreichend genug ist. Für den ausgewählten Detektor wurde die Winkelabhängigkeit untersucht und ein Kompensationsverfahren vorgeschlagen. Die Fähigkeit von ausgewählten Planungssystemen, reproduzierbare Behandlungspläne unter klinischen Bedingungen zu schaffen, wurde durch die Anwendung mehrerer Definitionen von Komplexitäts-Metriken ebenfalls untersucht.
Ein wesentlicher Teil dieser Arbeit widmet sich der Einführung zweier neuer komplementärer Software-Tools, die mit TomoTherapy-Einheiten, unter Verwendung der eingebauten Detektoren, angewendet werden können. Diese Tools ermöglichen es Benutzern, die Hauptursachen für Behandlungsfehler zu identifizieren und zu klassifizieren.
Darüber hinaus veranschaulichen wir, wie diese Programme genutzt werden können, um adaptive Strahlentherapie in der klinischen Routine zu implementieren, indem die Informationen genutzt werden, um die Maschinenleistung zu bewerten und anatomische Veränderungen zusammen mit ihren dosimetrischen Einflüssen zu untersuchen, sei es für einzelne Fraktionen oder kumulativ für die gesamte Behandlung.

Abstract

This work is dedicated to study the uncertainties occurring along the course of external beam radiation therapy.
At first it was tested and assessed whether the quality of the detector systems used to analyze uncertainties, as well as the rationale to decide if a plan is acceptable or not, is sufficient. The angular dependency was investigated for the selected detector system and a compensation method is proposed. The capability of selected TPS to create reproducible treatment plans in clinical conditions was examined as well by applying multiple definitions of complexity metrics.
A major part of this thesis was dedicated to introduce two new complementary software tools to be used with TomoTherapy units. These tools allow users to identify the leading causes for treatment failures using the built-in detector systems.
Furthermore, we illustrate how these tools can be implemented in an adaptive radiotherapy framework by using their information to assess machine output and anatomical changes together with their dosimetry influence on the therapy outcome of a single fraction or cumulatively.
Such methodical studies of the occurring uncertainties and their implications contribute substantially to the quality of treatments in radio-oncology centers.

Contents

List of Abbreviations

AAV Aperture Area Variability

ADA Angle Distribution Algorithm

ART Adaptive Radiotherapy

ASTRO American Society for Radiation Oncology

CF Correction Factor

CMW Cumulative Meterset Weight

CP Control Point

CT Computer Tomography

CTV Clinical Tumor Volume

DCS Dose Control System

DICOM Digital Imaging and Communications in Medicine

DQA Delivery Quality Assurance

DRD Dose Rate Drift

DVH Dose Volume Histogram

EPID Electronic Portal Imaging Device

GTV Gross Tumor Volume

H&N Head and Neck

IGRT Image Guided Radiotherapy

IMRT Intensity Modulated Radiotherapy

ITV Integrated Tumor Volume

IVD In-Vivo Dosimetry

kVCT Kilovoltage Computer Tomography

LINAC Linear Accelerator

LSV Leaf Sequence Variability

MCS Modulation-Complexity-Score

MF Modulation Factor

MI Modulation Index

MLC Multi-Leaf-Collimator

MU Monitor Units

MVCT Megavoltage Computer Tomography

OAR Organ At Risk

PTV Planning Target Volume

QA Quality Assurance

ROI Region of Interest

TPS Treatment Planning System

VMAT Volumetric Arc-Therapy

WHO World Health Organization

Chapter 1

Radiation oncology and its uncertainties

Soon after the discovery of x-rays by Wilhelm Conrad Röntgen in 1895, first medical applications of ionizing radiation were implemented leading to the first scientific publication related to radio-oncology in March 1897 (Freund (1897)).
Today, cancer is one of the leading causes of death in the world with about 14 million new cases per year and an expected increase of 70% in the coming 20 years (World Health Organization (2008)). New treatments are being developed while current techniques are constantly improved to ensure the best clinical outcome for each patient, to reduce the number of fatal cases, and to improve the quality of life after cancer.
Along with surgery, chemotherapy, and lately gene therapy, external beam radiotherapy is one of the main therapeutic approaches to treat cancer. The basic principle is the same throughout all applicable modalities: High energetic particles are projected towards the cancerous tissue in order to cause microbiological damage, e.g. strand breaks in the DNA, inducing apoptosis, a programmed cell death within our immune system. The goal is to eradicate the degenerated cells while sparing the surrounding healthy tissue. The latter poses a certain challenge, since ionizing radiation does not distinguish between normal and tumor tissue. On the one hand, it is vital to apply a sufficient dose to the target volume to stop uncontrolled cell growth. On the other hand, radiation must be applied as locally as possible reducing the dose to organs at risk (OAR) to avoid complications such as secondary cancers. A good compromise with little trade-offs needs to be found.
Although modern techniques provide good solutions to deliver a homogeneous and conformal dose distribution within the tumor, they cannot assure a 100% smooth progress of the treatment without any risks. Indeed, multiple uncertainties persist along the complete

treatment course, as illustrated in figure 1.1. The consequent errors influence the final result. In the best case scenario, the occurring errors might compensate each other, but in the worst case, they will add up. This may cause either overdosage - leading to side effects up to irreversible damage and death- or underdosage - leading to a possible relapse of the patient.

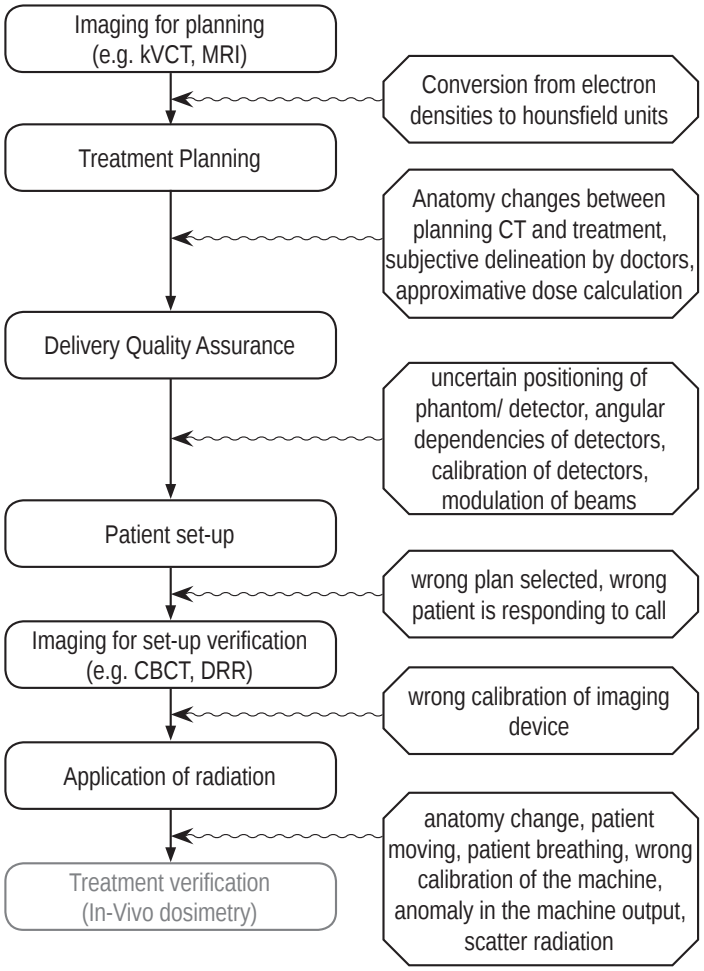

Figure 1.1: *The chain of radiotherapy (left) influenced by numerous uncertainties (right). The in-vivo dosimetry (IVD) is greyed out, since it is not applied by every center or with every technique.*

National and international organizations and institutions, such as ASTRO, AAPM, and EFOMP, have issued guidelines offering solutions and standard protocols in order to take into consideration the uncertainties at different levels of the treatment chain and to reduce the number of resulting errors.

At planning level, safety margins were introduced to mitigate the influence of small motion and anatomical changes. The first structure in the target area is the gross tumor volume (GTV), which is the actual size of the degenerated tissue visible on the scan. Knowing that the tumor has microscopic extensions not visible on the classical CT scan, an extra margin called clinical tumor volume (CTV) is added surrounding the GTV. Considering uncertainties due to statistical changes, e.g. patient's anatomy, an additional margin is created called planning tumor volume (PTV). Lately, another margin - called the internal treatment volume (ITV)- has been introduced to account for tumor motion, for example In lung cases.
In order to control the magnitude of uncertainties related to technical issues, for example the statistical fluctuation of the linear accelerator output and the progressive depletion of the electronic and mechanical parts. Several recommended quality assurance procedures are legally imposed, which ought to be done daily, monthly, and yearly (Klein et al. (2009)).
At delivery level, different technological advances have allowed to reduce uncertainties, such as imaging for patient positioning and tracking for patient motion. In addition, In-vivo dosimetry (IVD) verifications can be performed to control the quality of the treatment. Due to its benefits and capability of detecting both patient and machine related errors, IVD is enforced by law in numerous countries, e.g. in France (Institut National Du Cancer, (2008)), Sweden, Denmark, Norway, and the Czech Republic (Autorite de surete nucleaire (2014)).
Thanks to the additional information obtained by such techniques as IVD, a new approach of controlling the treatment quality was developed: Adaptive Radiotherapy (ART). In online ART, the treatment is verified and modified during the radiation delivery, whereas in offline ART, the delivery is assessed in between fractions and the remaining fractions will be adapted if necessary to reach the clinical goals.

The above mentioned procedures and the cumulated experience have given a certain assurance in the control of uncertainties, at least in the case of classical treatments. However, new techniques and technologies are developed to provide better treatment by increasing the accuracy and precision, i.e. the efficiency, of treatment delivery. By implementing new approaches, additional and yet unaccounted uncertainties are introduced, which need to be addressed.

This work studied such uncertainties that have not been accounted for at a state-of-the-art equipped center for radiotherapy.

Chapter 3 is thus focusing on the reliability of the measuring equipment on which assessments of uncertainties, the machine quality, and the technical capability of treatment delivery is being based. The investigation is focusing on using and correcting the angular dependency of a 2D detector in combination with rotational treatment techniques.
Chapter 4 is focusing on the planning software and its influence on the uncertainties and errors in radiotherapy by conducting a retrospective study on the level of complexity of rotational plans introducing several definitions of complexity metrics.
Furthermore, a new framework of In-Vivo-Dosimetry in TomoTherapy is introduced in Chapter 5, which might be used in a practical approach to implement adaptive radiotherapy. Considering figure 1.1, we are thusly investigating uncertainties at three principal milestones of a radiotherapy treatment: the quality assurance before the actual treatment delivery, performance of the linear accelerator during the delivery, and the verification of the delivery's quality retrospectively.

Chapter 2

Basic Principles of Radiotherapy

The basic principles and physics that serve as a foundation of medical physics in external beam radiotherapy will be discussed briefly in this chapter, starting with the creation of ionizing radiation and ending with the provoked microbiological effects and how it is used for medical purposes.
The interested reader is recommended to the following literature for more detailed information on basic principles of radiotherapy and radiobiology: Podgorsak (2005), Hall and Giaccia (2011), Khan (2009).

2.1 Ionization

The easiest approach in creating ionizing radiation is the use of radioactive isotopes with a long half-life. The element normally used in external beam radiotherapy is Cobalt 60 with a half-life of 52714 days (Khan (2009)) and a decay energy of round about 2.824 MeV with peaks in the gamma emission spectrum at 1.17MeV and 1.33MeV (Chofor et al. (2007)). First medical applications placed sources of ^{60}Co in a holder just above the patient.
Although ^{60}Co machines are still in use today, mainly in regions with a low GDP; most treating centers switched to linear accelerators. Their development allowed for a more compact design and thus affordable in price and housing for clinical centers.
The advantages over cobalt machines are the availability of higher and varying energies, different particles, photons and electrons, and the increased control of the radiation output, since it could be shut-off by pushing a button. That is possible due to the fact that their principle of creating radiation is not different to the classical x-ray tube:
Electrons from a source are being accelerated by oscillating electrical fields and are then guided towards a high Z material, e.g. tungsten. Penetrating the target, electromagnetic

interactions occur, such as deceleration of the electron (Bremsstrahlung), excitation of the target's atoms, which then fall back to their basic state (characteristic radiation), creating high energetic photons.

2.2 Biological Effects and Physics

When photons enter the tissue several energy dependent interactions with matter take place. The photon-effect dominates with lower energies, as the Compton-effect does with medium energies, and the pair production does with higher energies. For therapeutic energies (6-15 MeV) and human tissue, the Compton effect is the most important one (ct. figure **??**). That is why the energy received increases at first penetrating the tissue, since scattered electrons and photons are being produced creating a particle avalanche.

After a certain energy dependent depth an electronic equilibrium is achieved and the energy received decreases following the law of Lambert-Beer:

$$I_{(x)} = I_0 \cdot e^{-\mu x} \tag{2.1}$$

Where $I_{(x)}$ is the intensity at the depth x, I_0 the intensity before entering the matter and μ a material specific attenuation coefficient. In order to quantify "intensity", it might be useful to introduce the official unit being used in radiotherapy: the dose. Generally speaking, the dose is defined as the absorbed energy per mass unit:

$$D = \frac{\Delta E}{\Delta m} = -\frac{1}{\rho}\vec{\nabla}\vec{\Psi} \tag{2.2}$$

ρ is the electron density, Ψ is the fluence, number of particles intersecting a certain area, and ∇ is the nabla operator. The unit of dose is J/kg defined as Gray (Gy).
The higher the dose, the higher is the absorbed energy. This energy can lead to strand breaks in the DNA or the creation of free radicals poisoning the cell by breaking up the phosphorous backbone of the DNA helix. These effects aim at one goal: inducing the programmed cell death of the immune system, called apoptosis and other mechanisms.
Due to the degenerated state of the tumorous cells, the repair mechanisms are not as effective as with healthy tissue; hence, radiation is an efficient method to diminish the tumor. Since it is unavoidable to intersect normal healthy tissue, the difference in repairing efficiency is exploited by dividing the total prescribed dose to smaller amounts. By that fractionation, the tumor matter reduces, while the normal tissue can repair itself.
Other biological effects can also be used, for example the oxygen enhancement. Giving the

patient pure oxygen before the treatment leads to a fixation of the radiation damage, since free radicals of oxygen are creating bonds with the fracture of the DNA strand. Of course, this applies in general to tumors, who can have different oxygenation levels depending on their type of tissue.

2.3 Medical Application of ionizing particles

There are two main usages of ionizing radiation for medical purposes. One started already with their discovery by Wilhelm Conrad Röntgen, who saw that x-rays can traverse tissue, thus allowing imaging of biological structures. This feature is still used today in computer tomography (CT) and "normal" 2D x-ray images.
The second usage is radiotherapy. In early clinical linear accelerators (LINAC), the produced radiation was being collimated to a square field covering the area of the tumor delineated in the CT. Today, this technique is called "conventional radiotherapy". This led to the irradiation of larger volumes of healthy tissue in the vicinity of the tumor. The only way to avoid this was to adapt the shape of the beam to the form of the target tissue. That is why the "3D conformal radiationtherapy" was developed. Using this technique the unwanted radiation is being blocked by massive lead blocs and later by a device called multi-leaf-collimator (MLC). It consists of several movable plates of absorbing materials allowing to spare the organs at risk.
Following the evolution in computer technology, more complicated scenarios could be calculated in applicable time. That is why a new technique was developed, which considered the three dimensional extend of the tumor, the position of OARs to be spared and still create a homogeneous dose distribution within the tumor volume. For this technique, one needs to divide the beam into many several subbeams, called beamlets. Each beamlet can now receive a certain weight or proportion of the dose given by the LINAC from its particular angle. One needs to apply several irradiated surfaces having different shapes from the same angle to achieve this weighting procedure in reality. In doing so, one is able to modulate the intensity of each beamlet by irradiating its area several times or only once. Each irradiated surface contributing to the same beaming angle is called a segment. Due to the procedure's theory, the technique is called Intensity Modulated Radiationtherapy (IMRT). Applying several beams with several segments leads to a high tumor conformality while sparing critical organs.
Using IMRT for several years, the idea came up to use more beaming directions. The advantages are to spread the dose in order to spare the OARs even more, since parts of them receive smaller amounts of radiation. The problem was that accelerating the LINAC:

driving it to the next position, decelerate it to a full stop, applying irradiation, and again accelerating took too much time. The next step then was to get remove the "*step'n'shoot*" procedure, applying the radiation while the LINAC is moving. The so-called Volumetric Modulated Arc Therapy (VMAT) is exactly doing this. Basically, it is a 178 beam IMRT, where each beam consists of only one segment.
Advantages are the lower dose to the OARs and the plans are faster in application than normal IMRT plans. A single arc VMAT plan can be irradiated within two minutes, while the same plan quality in IMRT might take up to twelve minutes.
The increased speed brings several advantages with it. In a shorter time, more patients can be treated, allowing more people to be helped with their disease. Furthermore, it is better for the patient, since he or she has to lie down in an uncomfortable position for a shorter time. This additionally contributes to mitigating the uncertainty of patient positioning, since the patient does not start moving too much undergoing irradiation. Additionally, potential errors like choosing sub-optimal beam angles are being avoided, since the complete circle is used to deliver the planned radiation.

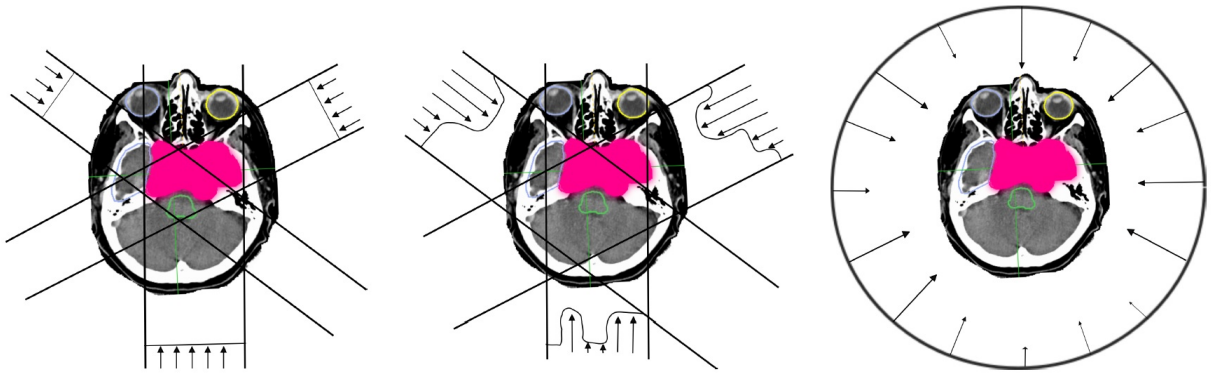

Figure 2.2: *Comparison of the three techniques. The arrows indicate the intensity. On the left the 3D conformal radiotherapy with three equally weighted beams. In the center IMRT using the same three beams but varying the intensity to spare the OAR (green structure). On the right VMAT, one rotating beam with different intensities.(Hofmann (2011))*

Another approach to deliver dose to a target volume was to use different particles. The first successful implementation is protons. Due to their electrical positive charge and mass, they produce different effects while interacting with the penetrated matter. The most relevant one is that their depth dose is described by the Bethe-Bloch-Equation, i.e. the energy transfer is proportional to the inverse particle speed squared. Thus, they have a low entrance dose sparing the normal tissue and a finite range (ct. figure 2.3), which is beneficial for OARs behind the target. In analogy, the development of photon

based radiotherapy, intensity modulated proton therapy, is introduced in clinical routine applying the same principles as IMRT, only with protons.

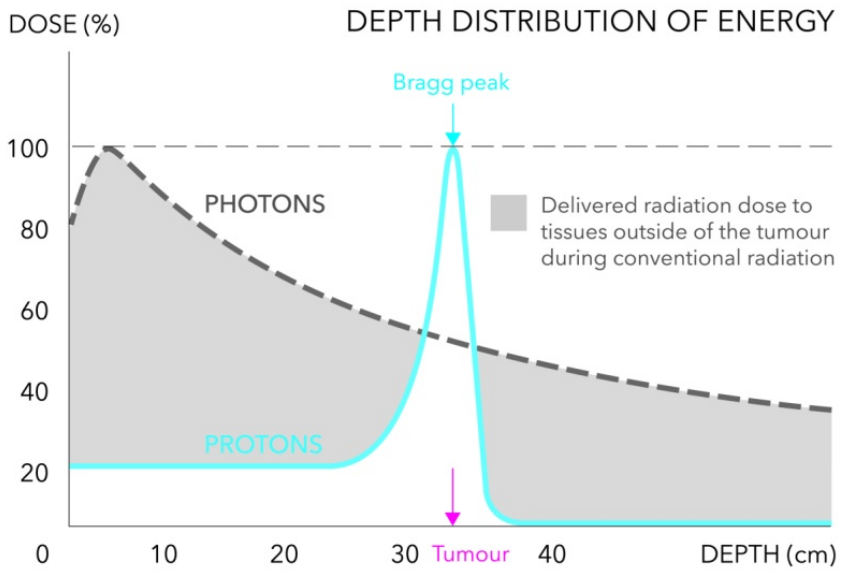

Figure 2.3: *Comparison of the depth dose curves of x-eays and protons.©Proton Therapy Center.*

Additional advantages like an increased biological effect lead to the interest in using heavier ions, e.g. carbon or oxygen (Dokic et al. (2016)). However, new and additional uncertainties were introduced with these particles; this issue will not be further elaborated since this work's focus is not on particle therapy.
All the presented approaches have in common that the plan is based on a certain central point, called isocenter, around which the LINAC is moving and the rotation is taking place in the same plane of this point, thus limiting the beaming directions and the degrees of freedom. One of the latest innovations in external beam radiotherapy is removing these constraints. It synchronizes the machine performance with the movement of the treatment couch and is called 4Pi (Dong et al. (2013)). The first results show a good conformal dose distribution within the target volume while better sparing the surrounding OARs.

2.4 Uncertainties and errors in radiotherapy

The development of external beam radiotherapy as described above aims at increasing the efficiency of irradiating target volume. These highly precise techniques depend on the following presuppositions: the optimal patient positioning, the coincidence of the anatomy and the images recorded by planning CT, flawless performance and output of the acceler-

ator, and the precise delivery of the calculated plan. But these factors are influenced by fluctuations and additional human failures. That is why it is concluded that an error must have happened when the delivered dose differs considerably from the calculated one. Such errors are subdivided in (van Herk (2011)):

- systematic errors
- statistical errors
- gross errors

2.4.1 Statistic and systematic errors

Statistic and systematic errors are inevitable and might be predictable or not. Their frequency and amplitude need to be evaluated, controlled, and limited. Predictable errors are quantified as the variability of the system being within the tolerance intervals of the applied method. The interval, in which unpredictable errors occur, is called uncertainty and can be numerically described by the standard deviations. The major uncertainties present in external beam radiotherapy are:

- Motion related uncertainties. The patient's anatomy is changing all along the treatment course and even during radiation delivery, due to, e.g. respiration or different amounts of bowel gas. As a result, the anatomy is not corresponding any more to the one of the planning CT, which is only a snapshot showing not moving structures.
- Patient positioning uncertainties. The patient has to be set up in the same position as in the planning CT. It is simply not possible to exactly reproduce the same position every day with the necessary precision. Safety margins are often used to compensate this issue.
- Uncertainties in contouring the structures in the planning CT, e.g. a misarranged definition of the target volume.
- Uncertainties of the accelerator.
- Errors in treatment planning and its delivery.

These uncertainties include two types of errors: systematic (initial patient positioning, organ segmentation, machine output) or statistic (motion, daily patient repositioning). Systematic errors affect the complete treatment. For example, the tumor volume was

contoured too small on which the whole plan and dose calculation is based or the systematic fluctuation of the machine output present at each fraction delivery. For all patients combined, systematic errors represent a smearing and a tendency. Statistical errors are anomalies of each fraction, like the small deviations of the patient position on the treatment couch. These punctual errors smear out over the numerous fractions of one single patient (van Herk (2004)).

The knowledge of systematic and statistical errors, especially of their magnitude, allows to consider them and to introduce counter-measures during planning and treatment delivery. Furthermore, safety systems allow, on the one hand, to verify that uncertainties do not exceed a certain threshold of acceptance, and on the other hand, to control process of treatment preparation and delivery.

2.4.2 Gross errors

Gross errors can be caused by material failure or human errors. They can be a consequence of being inattentive, intentional, or involuntary violation of existing protocols and procedures. Among the principle error sources are: issues with the equipment (including software), maintenance, calibration of the beam, treatment planning system, or even the parametrization and delivery of the treatment (Institut de Radioprotection et de Surete Nucleaire (2015)).

These errors might induce complications that can be gross, persisting, or even irreversible. An underdosage of the target volume decreases the tumor control probability and increases on the long term the risk of recidivisms. An overdosage can worsen the state of the patient considerably, causing necroses, ulcerations, bleedings, etc.

A safety report of the International Atomic Energy Agency (IAEA) mentions as well problems with the calibration, false usage of materials or the absence of adequate materials, and insufficient training of the staff. It stresses the importance of implementing a surveillance system at different levels of the treatment course (Agency (2000)).

Chapter 3

Uncertainties in the QA process: Assessment and correction of angular dependencies of 2D detector arrays

The assessment of the errors during any quality assurance verification relies on a previously measured database and an established standard.
As the Institut Curie, most modern radiotherapy centers use 2D chamber arrays for the quality assurance procedures. For these verifications, the users rely on the error tolerances and technical data provided by the manufacturer.
Nevertheless, additional verifications and adaptations of the database to the specific conditions of a radiotherapy center, individual treatment machines, and detectors may reveal hidden uncertainties. In fact, in the case of 2D arrays, it is vital to consider and verify the signal stability under changing angles, especially when doing a quality assurance of rotational techniques as with VMAT or TomoTherapy. Thus, it is crucial to verify whether the obtained results with the used detector are free of such influences, so one can actually trust the results of the QA verifications.
The angular dependency of 2D chamber arrays is a known issue (Wolfsberger et al. (2010)) and vendors themselves offer solutions for conventional c-arm accelerators (Shimohigashi et al. (2012)). In the case of the 2D chamber array MatriXX Evolution (IBA dosimetry GmbH, Schwarzenbruck, Germany) used at the Institut Curie, the solution consists of a set of correction factors for the angles from 0° to 180° with a step size of 5° in the ranges of 0°-50° and of 10° steps afterwards. In the most critical angles close to horizontal planes they are measured every 1-3°.
This observed angular dependency is caused by the different detection efficiency and cross

section of the chamber depending on the incident angle of the beam. Staying in the terminology of IMRT, one can imagine one bixel entering the active volume of a chamber orthogonally. Even with several chambers next to each other only the transversed chamber will fully detect the beam. Keeping the scenario but changing the incident angle to 90° the same beamlet will cross several chambers and the measurement will be affected as to the locality within the phantom.
One of the major problems leading to this effect is that the array and the LINAC are two independent systems. As such it is not possible to say which snapshot was taken at which gantry angle with sufficient certainty. In order to compensate this fact, manufacturers provide a gyroscope that can be attached to the gantry, continuously measuring the gantry angle and synchronizing it with the measured signals. The software then multiplies the measured snap with the corresponding correction matrix.
In addition, most vendors offer water equivalent phantoms into which the array can be inserted. Due to the geometry of the phantom the angular effects could be reduced (ct figure 3.2).

However, this modus operandi is not applicable in the case of DQAs performed with a MatriXX on a TomoTherapy unit. Due to the closed construction of such a unit (ct. figure 5.3) and the 360°of rotation, no device can be attached to the rotating gantry.
In this section an alternative workaround is proposed based on archived information in the treatment plan file.

3.1 Materials & Methods

3.1.1 2D detector array

As previously indicated, the 2D ionization chamber array is one of the most used devices in external beam radiotherapy treatment verification. Its advantages, amongst others, are the linear response of the chambers, independence on the hardness of the radiation, and as passive response detectors no extra process is necessary to obtain results. The used detector was IBA's MatriXX Evolution consisting of 1020 ionization chambers arranged on an equally spaced 32x32 grid with a center-to-center distance of 7.62 mm. The missing four chambers at the corners are virtually replaced by means of linear extrapolation by the vendor's readout software. A 100% covering dose distribution is achieved by linear interpolations between neighboring chambers.
These chambers are air-vented and possess a minimal 20ms read-out time. Their diameter

is 4.5mm and with a height of 5mm creating a measuring volume of 0.8cm^3.
If needed a gyroscopic sensor (ct. figure 3.1)can be attached to the Gantry. By that the corresponding angle of each measurement snapshot, hereafter called snaps, can be recorded. The interval between two snaps can be adjusted by the user and is defined as the sample rate. The rate throughout this work is set to 500ms. If necessary the snaps can be exported as txt-files and even be re-imported.

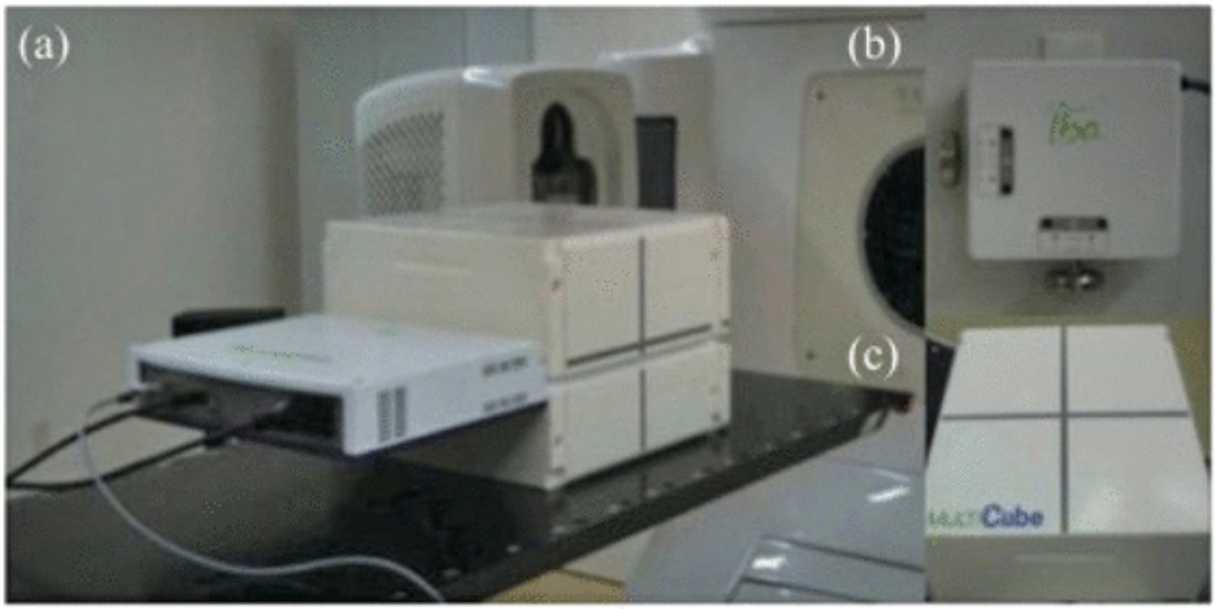

Figure 3.1: *On the left the MatriXX detector inserted into the Multicube phantom (a) is shown. The compatible attachable gyroscopic sensor for determining the gantry angle is depicted on the right(b). Under the gyroscope the MultiCube (c) is shown without the MatriXX. ©Shimohigashi et al. (2012)*

In order to gain electronic equilibrium in the measuring plane and to reduce disturbing back scattering from the penetrating radiation the array can be inserted into a cubic phantom called MULTICube. It is made of a special plastic having the same electronic density as water, thus being easier to be considered in dosimetric calculations. Publications indicate that its design (ct. figure 3.2) is minimizing the angular dependency of the detector as well (Xu et al. (2010)), which will be analyzed later in this thesis.
The MatriXX is connected to the software OmniPro I'mRT (v1.7.0021), which was also used to compare the corrected and uncorrected measurements.

Figure 3.2: *The multicube phantom with the MatriXX detetctor inserted is shown on the left. The right image demonstrates the same phantom with a setup allowing the insertion of a film without having an air gap. (IBA Dosimetry GmbH (2009))*

The background was measured directly before starting each measurement to account for signal noise from, e.g. cosmic radiation, so that it could be subtracted immediately. Additionally, a warm-up time of 15 minutes was considered.

3.1.2 Film dosimetry

2D arrays like the MatriXX are successors of older 2D dosimetric measuring tools but still possess certain disadvantages. The two most relevant points are the angular dependency and the spatial resolution caused by the finite dimensions of the ionization chambers. That is why, despite their long history, passive detectors like radiochromic films are still being used, especially for small field dosimetry where other detectors do not perform well. Hence, it was decided to use results obtained with film dosimetry as a reference.
The chemical composition of the thin films is reacting with, e.g. ionizing radiation, leading to the creation of polymers that become opaque. The opacity is proportional to the dose received, although it is not in direct linear correlation. For that reason, a so called calibration curve needs to be measured. The curve is measured by irradiating a film with several known doses, so that one is able to assign a certain optical density to a specified dose (ct. figure 3.3).
Today's EBT3 films, also called gafchromic, are self-developing films that don't need chemical processing like their predecessor the EBT1. Nevertheless, it is important to introduce a specific protocol due to the chemical reaction, and as such the darkening is taking place several days until it stabilizes.
In this work two different protocols were used due to an installation of a new scanner:

1. The films were scanned 18 hours after irradiation, like the calibration curve. Due to the inhomogeneous light distribution of the scanner lamp, the films were always digitalized in the same orientation as the calibration. Additionally, the films were placed in the center of the flatbed, were the most homogeneous light was found.

2. Caused by the installation of a new scanner, a new calibration curve was created based on films that were scanned 16 hours and 30 minutes after irradiation. Thus, the measuring protocol was adapted accordingly.

The scanner used with the first protocol was an Epson 3000 and for the second one an Epson Expression 11000XL. Both are usual flatbed scanners and their scanned images are saved in the TIFF format. The evaluation was done with the software FilmQA Pro version v4.0.50399.34122. It can import the scanned images and helps to evaluate the results.

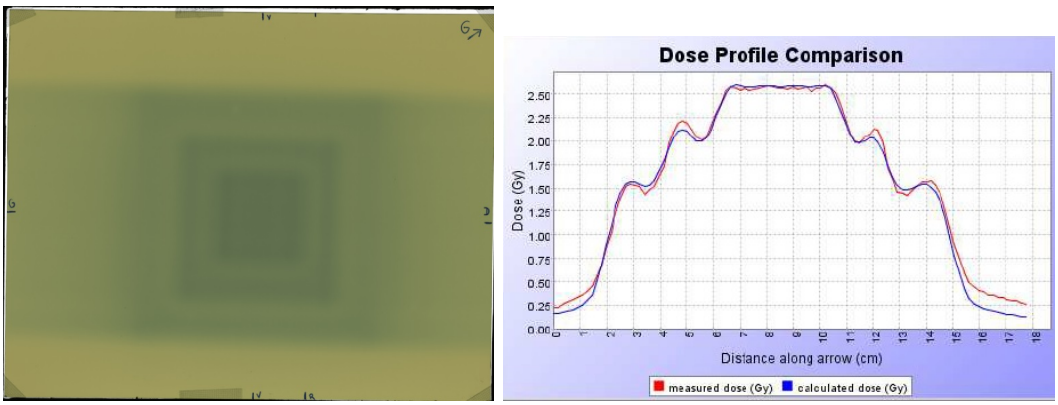

(a) Scanned film (b) Profile in longitudinal direction

Figure 3.3: *Example of a calibration measurement. The film was irradiated with different field sizes and different doses, thus creating a 2D projection of pyramid. The square at the center received the most dose as it is being irradiated three times and then going outwards the dose decreases.*

The biggest disadvantage of films is the increased workload even with self-developing chemicals. One still has to scan each film after waiting for the time as previously used for the creation of the calibration curve. In addition, you need to recalibrate the dose-to-optical-density curve for each new badge of films, since small changes in the chemical composition might have a non-negligible influence on the darkening process.

3.1.3 Gamma analysis

One method to classify the quality of a dose delivery is widely used in radiotherapy QA: It is called gamma analysis (Low et al. (1998)) and compares the actual delivery to the

planned dose distribution. Being aware that a dosimetric deviation can be created by a slight misplacement a gamma analysis is considering the dose at a given point within its environment. That means if at the investigated point the expected dose is different to the planned one and only slightly shifted by a few millimeters, it can still pass the test criterion. The gamma criterion is specified by two values: the dose difference and the distance to agreement, both usually noted like 2%/2mm. It implies that a dose difference of 2% within a 2mm radius of the analyzed point is accepted.
Since there are thousands of pixels to consider in a dose distribution, it is stated that a certain fraction of the pixels, e.g. 95%, should fulfill the criteria. This value is usually called the passing criterion.

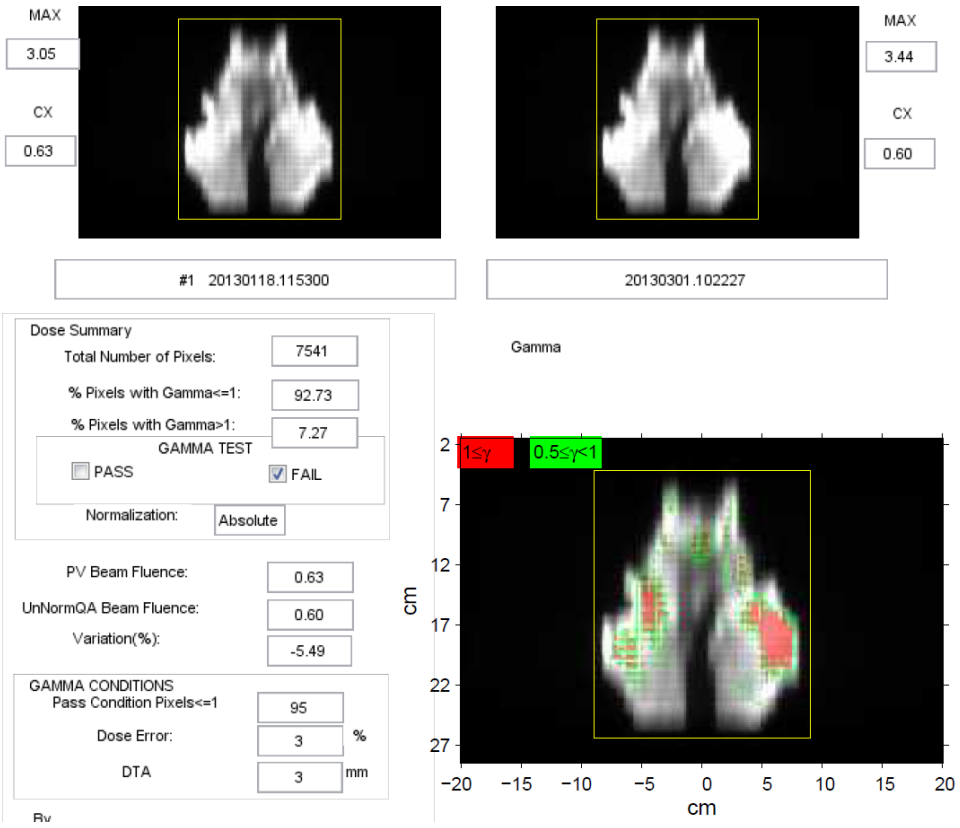

Figure 3.4: *Example of a gamma report. Shown above are the planned dose distribution (left) and the measured one (right). In the lower left corner is a summary showing how many pixels in total were analyzed and how many of them passed (92.73%)/ failed (7.27%) the criterion in percent. The applied criterion is shown below in the box "GAMMA CONDITIONS". 95% of the investigated pixels should have a dose difference lower than 3% within 3mm. On the lower right is the corresponding visualization of the analysis. The red areas mark the failing pixels and the green the passing ones. The uncolored areas have a gamma value below 0.5.*

Due to the wide acceptance both, OmniPro I'mRT and FilmQA Pro, provide the possibility to calculate a gamma analysis. Thus the passing rates will be compared to evaluate the results of the correction method. The passing criterion is set to 95% for a gamma criterion of 3%/3mm.

3.1.4 Symmetric response of the detector and qualification of the angular dependency

A preparatory test was conducted to exclude the influence of a potential intrinsic asymmetry of the 2D detector. The test was performed on a Varian 2100 C/S linear accelerator with an energy of 6MV and a dose of 100MU for each field. The field size was set to 40cmx40cm in isocenter to cover all 1020 chambers.
The MatriXX was inserted into the MultiCube phantom to account for the build-up effect and backscatter radiation and to recreate the setup of actual QA measurements. The field was then irradiated from various gantry angles: 0, 60, 70, 80, 85, 90, 95, 100, 110, 130, and 145. These angles were completed by their mirrored values to test the symmetry. The stepsize was decreased in the interval (80,100), since it is expected to find the biggest angular effect at these angles.

3.1.5 Influence on the measurements of the divergence of the beam

Next, it was tested whether the influence of the gantry angle applies to all chambers in the same magnitude, as it is proposed by some commercial solutions. Considering a homogeneous environment with a uniform dose distribution, the angular effect was quantified by dividing the measured value of every single chamber by its value as calculated by the TPS. Showing all 1020 graphs of the obtained results would not be helpful to understand the mentioned problem. That is why the following eight chambers were chosen to represent the results, since they show the two extremes in terms of the effect created by the beam's divergence:

- The four central chambers (please note that the MatriXX has no central chamber), denominated P1-4.
- The four corner chambers, P5-8.

The exact coordinates of the eight points with reference to the MatriXX's center are: P1(-0.38,0.38), P2(0.38,0.38), P3(0.38,-0.38),P4(-0.38,-0.38) and P5(-12.19,12.19), P6(12.19,12.19), P7(12.19,-12.19), P8(-12.19,-12.19)

3.1.6 Correction Factors

In order to assess an angular correction it is necessary to know its magnitude. Having shown that it is important to consider the position of the chamber in relation to the field, two separate sets of correction matrices were investigated. These sets of matrices result from two different methods of creating the correction factors: either empirically by comparing the array's measurement to a reference detector or by calculating the detector response, e.g. with Monte Carlo simulations.

3.1.6.1 Obtaining correction factors using cross-calibration with film dosimetry

Based on the fact that the vendor's correction matrices for the used MatriXX model apply only one factor per angle for all 1020 ionization chambers, ignoring the beam's divergence for off-axis chambers, it was decided to create a new set of matrices obtained by cross calibration with EBT3 Gafchromic films (ct. chapter 3.1.2).

To achieve this goal a protocol was developed in which static gantry procedures of a TomoTherapy unit were created at various angles. The same procedure was then irradiated twice: Once each on the MatriXX detector in the MultiCube and as well as on the film with its special insert to ensure comparability of the results. The insert is filling the air gap, since a film is thinner than the 2D array. In addition, the insert ensures that the film is at the same height as the measuring plane of the MatriXX's ionization chambers. The correction factors are obtained from the superposition of the MatriXX's results and the EBT3 results by applying:

$$CF_{ij} = \frac{D_{ij}^{MatriXX}}{D_{ij}^{Film}} \tag{3.1}$$

Where i and j are row and column indexes of the center position of the chambers and D the measured dose. In order to create a full set of correction matrices and a better approximation of the needed correction, the obtained results were mirrored and used as fixing points for linear interpolations. By doing so a step size of 1° could be reached, i.e. a set of 360 correction matrices was created.

3.1.6.2 Using the manufacturer's correction factors

The official CFs were included in the study although they neglect the effect on the off-axis chambers and were created solely for open fields (20cmx20cm). Nevertheless they are accepted as an official solution applicable in a clinical environment. Their values are presented in figure 3.5. They were calculated by modeling the chamber responses in Monte Carlo simulations.

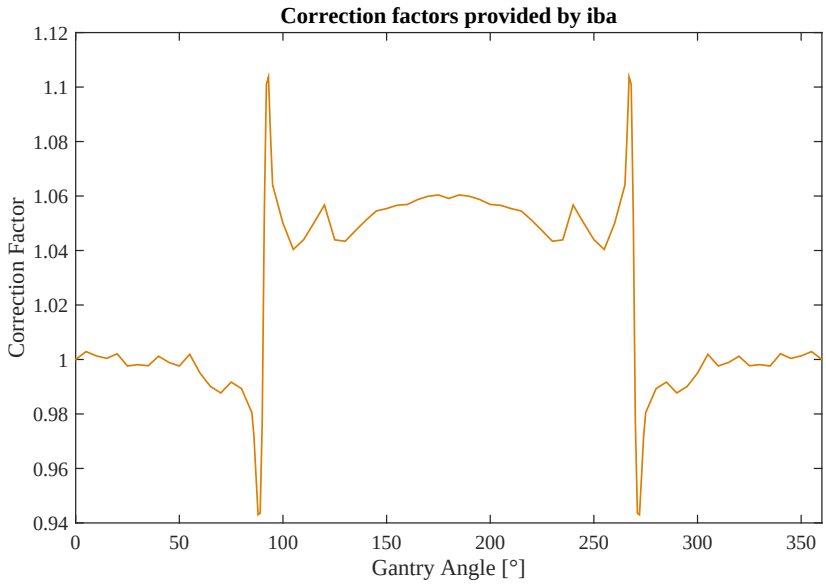

Figure 3.5: *Correction factors extracted from the matrices as provided by IBA to be used with the gyroscopic sensor on "conventional" linear accelerators.*

As in chapter 3.1.6.1 the provided factors are mirrored and linear interpolated to increments of 1°.

3.1.6.3 In-House developed correction algorithm

The first and main problem is to find the gantry angle corresponding to each snap, since the gyroscope cannot be used. Thus the presented approach is introducing a virtual gyroscopic sensor. The created algorithm uses the recorded plan data of the DQA which is stored in a XML file and can be retrieved by archiving or exporting the patient files. The necessary information is to be found in the personalized file with the scheme FAMILYNAME^FIRSTNAME_*patient.xml*. Opening the file it is important to search the first "Treatment" position, otherwise the information of the MVCT for positioning will be loaded, which is different in its characteristics to the ones of the treatment e.g. less

projections per rotation. In addition, it is necessary to check if the process has finished successfully, otherwise the information will be false or incomplete. The status is indicated by the missing "Interrupted" entry in the "treatmentProcedure". Now the actual information can be extracted, namely the "nominalGantryPeriod", "desiredGantryStartAngle", "deliverTimeSeconds", and "deliverTime100USeconds". The variables are self explanatory, but it should be pointed out that 100USeconds represent 100μs leading to the total delivery time in seconds: $t_{total} = deliverTimeSeconds + deliverTime100USeconds \cdot 0.0001$.
The gantry speed in $^\circ/s$ can now be calculated with $\overrightarrow{v}_G = \frac{360^\circ}{nominalGantryPeriod}$.
The first idea right now would be to delete all first zero-snaps, since the measurement can be started at any moment independently of radiation being present or not, and assign the desired gantry start angle to the first snap and then start to count. However, this approach will probably lead to false results, because the TomoTherapy® unit is starting the radiation a few seconds and degrees before this value in order to provide the planned dose and dose rate at the first saved position. This might lead to a recorded non-zero snap not being at the programmed start angle.
The gantry angle at which radiation starts is calculated from the gantry angle at which radiation stops, corresponding to the last non-zero-snap, as shown below:

$$\vartheta_{lastProj} = desiredGantryStartAngle + (t_{total} * \overrightarrow{v}_G) \ \% \ 360 \tag{3.2}$$

with % being the modulo operator.
Knowing the sample time of the MatriXX, 500ms in this study case, it is possible to count backwards until the snap of the desiredGantryStartAngle has been reached. It can be found by calculating the number of irradiated snaps: $S_{irr} = \frac{t_{total}}{Sampletime}$ and counting backwards as well.
Now, the software is ready to correct the measurement by extracting the 32x32 chamber signals exported in TXT format by the evaluation software. These values are then multiplied with their corresponding correction factor and again exported in TXT format, so they can be re-imported to OmniPro I'mRT for further analysis.
The flowchart summarizing the program is shown in figure 6.1.

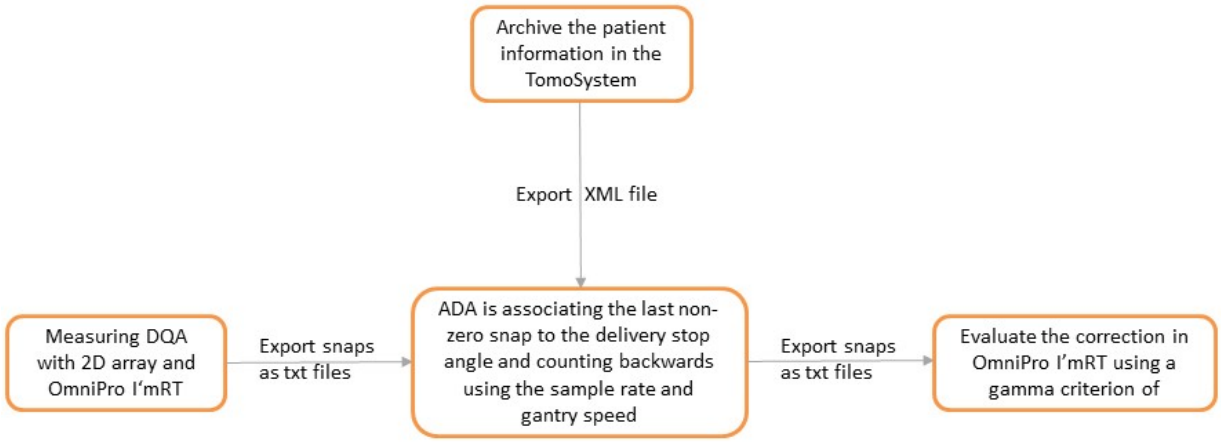

Figure 3.6: *Workflow of the angular correction using a 2D detector array.*

In order to test this approach, eleven clinical cases were chosen and re-irradiated. The gantry angle of each dose projection was extracted from the Tomo-System directly after the application of the irradiation. The data was then analyzed and the angles of the projections at 0%, 25%, 50%, 75%, and 100% of the process of the plan extracted and compared to the values calculated by the angular distribution algorithm (ADA).
28 clinical cases with the following treatment sites were tested to verify the complete algorithm, including the correction factors: one opthalmologic, two anal canal, three rectum, two lung, two lumb (leg), two breast, seven gynecological, and nine head and neck cases. The selection was done arbitrarily among the newest DQAs. It was decided to incorporate more gynecological and head and neck cases, since they are usually more complicated to be irradiated. Due to their complexity a high modulation is to be expected and as such a high number of beaming directions, which should increase the effect of the angular dependency. The results of the correction will then be compared to the uncorrected ones using OmniPro I'mRT by applying the above mentioned gamma criterion. In order to exclude false negatives or false positives, the cases with the biggest differences in passing rates were remeasured using radiochromic films as a detector to have the corresponding reference value.

3.2 Results

3.2.1 Symmetric response of the detector

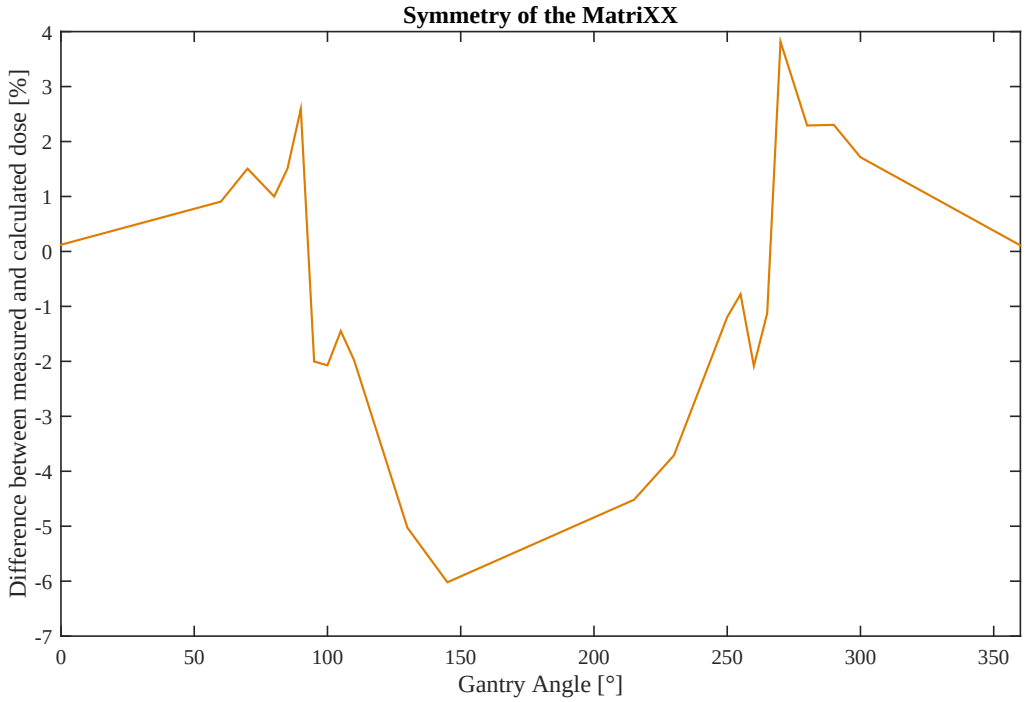

Figure 3.7: *Results of the test if the MatriXX has intrinsic asymmtries for the four central chambers.*

The measurements, as shown in figure 3.7, confirm a sufficient symmetry of the 2D array. This allows to assume that the structure of the detector itself does not have an influence on the signal response. Only the peak values at 90° and 270° show a slightly asymmetric behavior. It can be explained by the table's construction and an additional backscatter plate integrated in the 2D array protecting electronic parts. Alternatively, the factory array calibration may also play a role.
The obtained result confirm the findings of Wolfsberger et al. (2010) and the actual presence of the angular dependency.

3.2.2 Influence on the measurement of the divergence of the beam

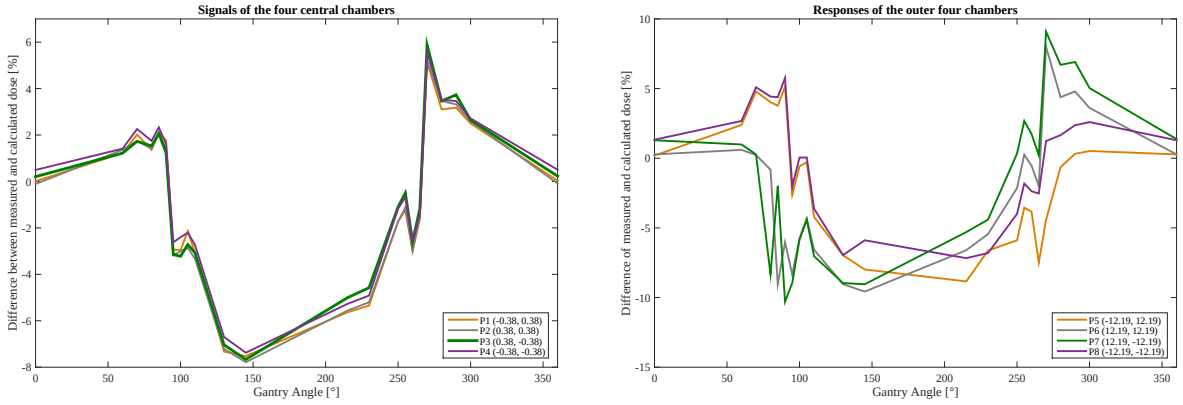

(a) (b)

Figure 3.8: *Signals of the four central chambers, P1-P4, (a) and the four on the outer corners, P5-P8 (b). While P1-P4 have an almost parallel behavior showing that the divergent effect is negligible at these positions; one can see that there is a discrepancy for P5-P8. One can even determine which chambers are on the same side of the gantry. The coordinates with reference to the MatriXX's center are given in cm in the legends.*

It can be seen in figure 3.8 that while the four central chambers are responding in a good symmetry, the four outer signals prove a strong non-negligible effect. Differences in signal response go up to 16.07 percentage points at 90° and 12.43 at 270°. It can be observed that the angular influence is stronger in lateral than in longitudinal direction, which can be explained by the change of the incident angle of the beam when turning the gantry. The results show that it is necessary to have more than one correction factor for all chambers per gantry angle to obtain more accurate results.

3.2.3 Correction factors obtained by cross-calibration

The obtained results of the four central chambers are shown in figure 3.9 together with the vendor's CFs.

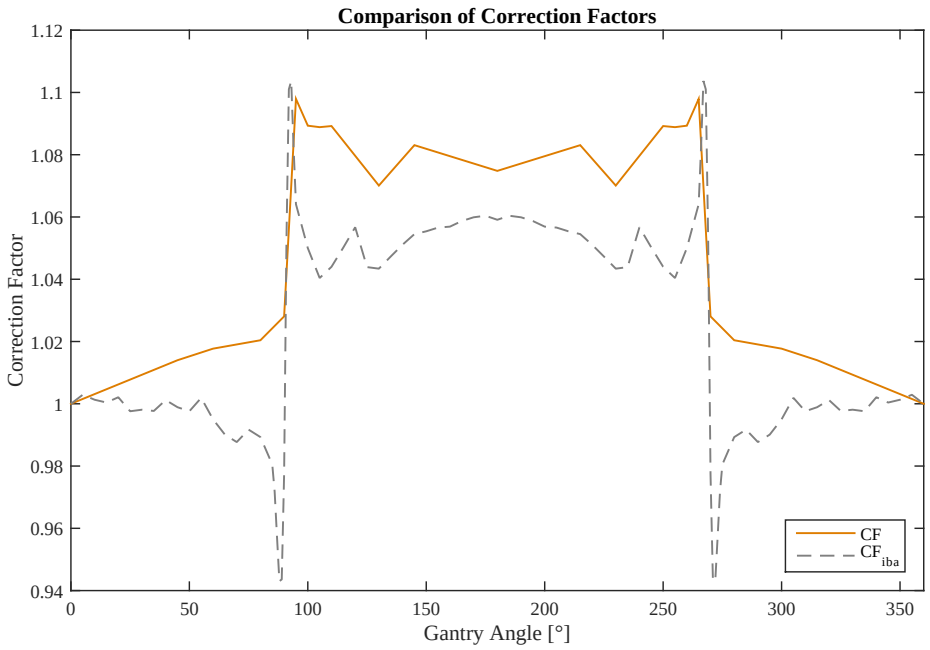

Figure 3.9: *Results of the CFs of the four central chambers obtained by the cross-calibration with Gafchromic films (solid, orange line) in comparison to the CFs provided by IBA (dashed, grey line).*

The self-created CFs display an interesting behavior. Instead of decreasing in the intervals (0°, 95°) and (360°, 270°), they are constantly increasing. The minimum of IBA's factors had been missed due to our step size indicating that in this range one should measure in 1° increments.
Additionally, the values in the interval (95°, 270°) are in average 2.47% higher than the official commercial correction. The resulting DQA checks, which can be found in chapter 3.2.5.1, showed that the factors lead to lower gamma passing rates than the original uncorrected measurement.

3.2.4 Angular distribution algorithm

Table 3.1 is showing the results of the Angular Distribution Algorithm's (ADA) verification taking the average of all tested cases.

Table 3.1: *Differences between the planned gantry start angle and the recorded value of the first dose projection, and the recorded gantry angles of each projection and the calculated ones for the specified point of progress of the treatment. The results show the average of all test cases including their standard deviation.*

Process of the plan [%]	$\Delta\theta_{GantryStart}[^\circ]$	$\sigma_{\Delta\theta_{GantryStart}}[^\circ]$	$\Delta\theta_{Snap}[^\circ]$	$\sigma_{\Delta\theta_{Snap}}[^\circ]$
0	3.46	0.05	3.42	2.74
25	N/A	N/A	46.84	87.21
50	N/A	N/A	4.03	3.07
75	N/A	N/A	4.09	2.26
100	N/A	N/A	3.21	1.05

The differences between calculated and recorded gantry angles match within 4.09°, which is slightly higher than the difference of the planned starting angle and the first recorded gantry position, which is 3.46°. Additionally, it is smaller than 5° and as such smaller than the distance between two fixing points of our linear interpolation. Keeping in mind that any angle could be possible, the achieved accuracy is in the range of 1.14%. Thus, it is assumed that the ADA is working with an acceptable accuracy.
The only erroneous results were obtained with two head and neck cases. One was off by -165.02° and the second one by -170.04° at the 25% progress point. A reason for this behavior could not be found yet. The distribution of the dose projections over all four quadrants of the circle were similar to the other plans and there was no other value, e.g. gantry period, dose projections per rotation, gantry start angle, or prescribed dose, distinguishing these two cases from the rest. It might be possible that the synchronization progress did not work in these cases due to a problem during the delivery of the DQA. A bigger sample size in the future might uncover the reason for the failure at the 25% position.

3.2.5 Application of the angular correction on clinical cases

3.2.5.1 Film based correction factors

Looking at the final results, the apparent differences between the vendor provided factors and the obtained results from chapter 3.2.3; it was expected that the proposed correction will constantly lead to lower passing rates. Thus, only a few of the above mentioned cases were tested to prove that the correction factors obtained by the cross-calibration should not be used.

Table 3.2: *Results of the DQA measurements corrected with the film based CFs applying a 4%/3mm gamma criterion. Serving as a comparison the values of the vendor based corrections are shown as well.*

	Uncorrected DQA [%]	Film based CFs [%]	Vendor based CFs [%]
H&N 1	95.97	90.58	99.47
H&N 3	99.05	94.52	99.92
H&N 4	99.88	95.04	99.49
H&N 8	99.38	95.62	99.7
Rectum 1	100	97.87	99.79
Gyneco 2	99.76	80.16	99.53
Canal Anal 1	99.76	85.74	99.43

As one can see the applied CFs result in lower passing rates throughout. In some cases even to the extent that the plans fail the passing criterion. Even though, the manufacturer based results show improvements or are in the same range, within 0.5%, as the uncorrected acceptable results and are shown for comparison in the table as well.
Reasons for the differences will be discussed later on.

3.2.5.2 Manufacturer based correction factors

As shown in figure 3.10 the applied correction with the vendor based CFs produce in general better DQA results or at least in the same range, i.e. the average difference excluding the big deviations is 0.05 percentage points. The correction gave worse results only in the case of Gyneco 6. These results cannot serve as a final proof of whether the presented approach works successfully or not, since false positives or negatives can be created by the angular effects.

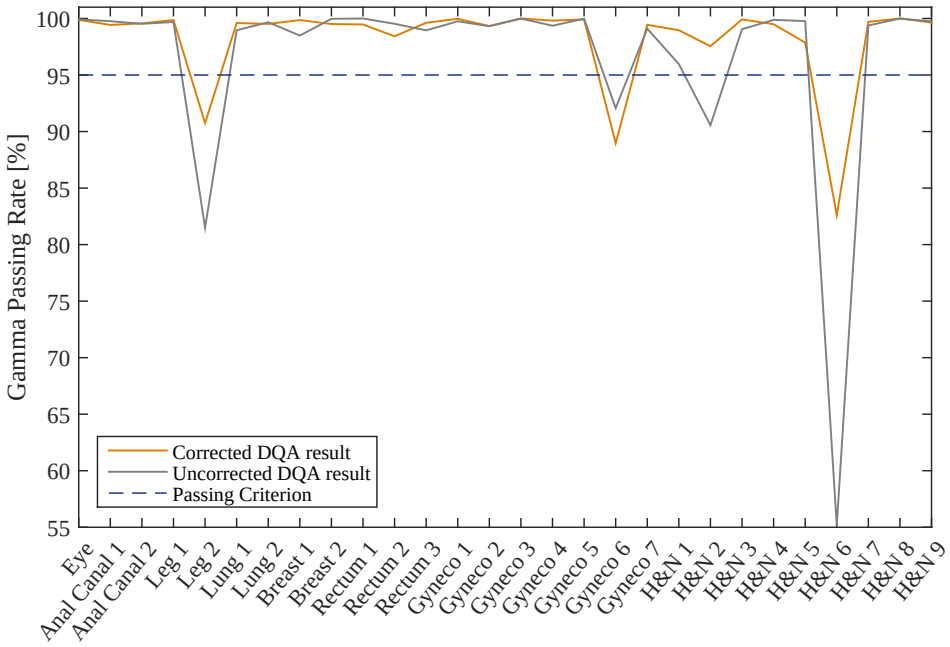

Figure 3.10: *Comparison of the DQA results uncorrected (grey) and corrected (orange) for the angular dependency of the MatriXX.*

In order to verify which of the results are a better representation of the reality, the cases with the most pronounced differences were chosen and remeasured using Gafchromic film as a reference with a newly installed scanner. The results of the control are shown in table 3.3.

Table 3.3: *Verification of the DQA results. EBRT3 Gafchromic films served as a reference to decide which value is to be interpreted as the correct one. The film of leg 2 could not be analyzed due to an unknown software issue.*

	uncorrected DQA [%]	corrected DQA [%]	film DQA [%]
H&N 6	55.16	81.63	84.33
H&N 2	90.56	97.55	97.4
Gyneco 6	92.07	88.97	100
Leg 2	81.49	90.74	N/A

It is difficult to derive a clear conclusion from the verification, since there are only three interpretable results. For the cases H&N 6 and H&N 2 it is clear that the corrected measurements match the film DQA's passing rate very well, whereas for Gyneco 6 the uncorrected measurement is closer to our reference, although it has a non-negligible difference of eight percentage points.

In the leg 2 case it was not possible to load the scanned film into the evaluation software. It was scanned several times to exclude a corrupted file and remeasured a week later, but still the software refused to load the image. Since it was a leg case having the primary dose distribution very far off-axis, it is assumed that the software had problems with the coordinate system.

3.3 Discussion

The presented approach shows the necessity of considering the angular dependency in QA processes based on the information obtained with a 2D chamber array, as such as the one evaluated in this work, the MatriXX. For correcting measurements it is necessary to apply correction factors to the raw measurements.
Two different sets of CF matrices were tested and compared. The set based on the cross-calibration with film dosimetry lead to lower passing rates than the uncorrected results. This is caused by the CFs themselves, which have large differences to the official and commercial available correction matrices. The scanner's quality might have influenced the results of the film measurements as the reproducibility of the films was not as expected. In fact, a later investigation showed that the same film scanned several times lead to up to 5% difference in signal.
The factors provided by IBA though lead to good results and in general higher passing rates than the uncorrected measurements. One might be surprised, since the vendor's CFs do not consider the divergence of the beam and as such ignoring the effect on the off-axis chambers. An explanation is the nature of rotational techniques: In order to decrease the dose to the normal, healthy surrounding tissue a high number of beams is delivered in small portions leading to small field sizes and as such to small bixels contributing to a segment. Thus, the divergence is rather small. If the plans consisted of large open fields, these factors would probably also lead to lower passing rates.
IBA itself noticed that the set of the correction factors need to be improved. The new generations of MatriXX detectors are delivered with new sets based on Monte Carlo simulations. Due to the different intrinsic structure these are not applicable for older models. A comparison between corrected and uncorrected DQAs show the same magnitude improvement as our results (ct. figure 3.11).

Plan Details	Full rotation		Gantry 0°
	Without angle correction	With angle correction	
HN 6MV dMLC	88.4	99.8	99.61
HN 6MV dMLC FFF	95.7	99.9	99.6
HN 6MV dMLC	68.9	99.4	98.9
HN 6MV VMAT FFF	92.7	99.8	98.0
Prostate 6MV dMLC	71.6	98.3	99.1
Prostate 6MV dMLC FFF	79.0	97.9	99.1
Prostate 6MV VMAT	78.6	99.6	99.1
Prostate 6MV VMAT FFF	88.9	98.7	99.1
HN 10MV dMLC	66.4	95.1	98.4
HN 10MV dMLC FFF	97.6	99.1	99.6
HN 10MV VMAT	52.7	95.7	95.3
HN 10MV VMAT FFF	99.4	99.4	99.6
Prostate HF-1 VMAT FFF	99.5	96.43	100
Pelvis HF-2 VMAT FFF	80.0	99.28	99.2
Lung HF-3 VMAT FFF	62.4	99.8	100.0
Lung HF-4 VMAT FFF	98.7	97.12	99.4
HN HF-5 VMAT FFF	95.6	99.71	99.7
HN HF-6 VMAT FFF	95.2	98.9	99.5

Figure 3.11: *Angular correction using the CFs provided by IBA with their new detector generation. (Sekar et al. (2016))*

In order to apply the correction factor to the corresponding snap, it is necessary to know the gantry angle of each snap. An algorithm was developed which is replacing the physical gyroscopic sensor by a virtual one relying on the machine data from the plan file. The verification of the ADA shows its capability of accurately determining the gantry angles of the snaps by counting backwards from the last dose projection.
The only two exceptions were two head and neck cases at the 25% position of the treatment where both are off by more than -160°. Although a thorough investigation was launched the reason for this difference could not be found yet. A bigger sample size might uncover the distinctive factor of these cases.
The verification of the corrected results with the film detectors serving as a reference showed a good agreement with our findings which are comparable to the results in figure 3.11.

The major insecurity of the presented approach is still the synchronization of the gantry angle and the snaps, since the ADA is a theoretical calculation, which cannot consider deviations occurring the DQA delivery. Thus, it would be better to introduce a system

that actually can detect the gantry angle of each dose projection. An example of such a system will be discussed in chapter 5.7.

A positive effect is that stricter gamma criteria might be applied to already detect minor problems that would have remained undetected without the correction of the angular effects. A first small study of a gamma criterion of 2%/ 2mm is shown in table 3.4. Canal Anal 1 is such a case. With a gamma criterion of 3%/3mm the passing rate was 99% for the uncorrected and 97% for the corrected one. Penalizing smaller changes with the new gamma criterion, the passing rate is dropping to 76.72% indicating a potential problem.

Table 3.4: *Preliminary results of a first sensitivity study if a stricter gamma criterion of 2%/ 2mm might be used after the correction of the angular dependency.*

	Uncorrected DQA [%]	Corrected DQA [%]
H&N1	69.36	83.02
H&N3	88.34	92.66
H&N4	91.03	91.11
H&N7	85.95	88.92
Rectum 1	97.43	92.21
Canal Anal 1	71.1	76.72

Having the reduced uncertainty of angular dependency using a 2D chamber array, it is possible to further analyze other uncertainties applying this kind of detector.

Chapter 4

Uncertainties in VMAT QA and delivery due to modulation. A theoretical retrospective review

One of the most popular techniques in modern radiotherapy is VMAT, as discussed in chapter 2. This technique involves a constant motion of the gantry while delivering an intensity modulated treatment plan. The delivery of such a plan is highly complicated as the leaves of the MLC are constantly adapting their shape while staying synchronized to the beam angle.

Multiple factors have to perfectly interplay to create an acceptable dose distribution. These parameters, to be adjusted during the treatment delivery, are: the gantry angle, the gantry speed, the dose rate, the position, the speed of the leaves of the MLC, and lately the treatment couch position. The change of their values leads to a stronger, more complex modulation of the dose. The stronger the change of the values, the higher is the modulation of a treatment plan. In comparison to IMRT many additional variables are to be considered introducing more uncertainties. Only one of these factors malfunctioning could already lead to a treatment error.

At our center, it was observed in clinical routine that a higher than usual amount of plans fail the quality assurance check prior to the actual treatment. After excluding the most typical sources of errors like sharp dose gradients or failure of the measurement chain, it was suggested that the discrepancies might be due to a high level of modulation. In its struggle to achieve the planning requirements, the TPS could overmodulate, i.e. calculate a theoretical plan with such parameters that cannot be achieved in real treatment conditions within an acceptable tolerance (Kruse (2010), Hanusova et al. (2015)). The modulation

itself and its constraints are dependent on the used TPS, since each vendor has his own way of dealing with the plan optimization.
Although the manufacturer has implemented safety algorithms which should theoretically prevent this from happening (Yang et al. (2015)), this occurrence has been reported in- and outside our department. However, previous investigations of the phenomenon remained inconclusive, since literature is indicating both: the modulation is either affecting the DQA (Masi (2013)) or not (Celi et al. (2015)). An investigation was launched to officially confirm or deny the suspicion for VMAT cases at our center. In the case of confirmation the implemented tools could be used as a predictive warning system.

4.1 Materials & Methods

4.1.1 C-arm LINACS

Due to their long history and technological evolution allowing for isocentrical treatments, c-arm shaped linear accelerators are the most used devices to deliver external beam radiotherapy. The accelerators used in this work are a TrueBeam (Varian medical systems) and a 2100 C/S (Varian medical system). Both machines are capable of delivering rotational treatments, like VMAT. They are operating with different energies for photons and electrons at various dose rates and are equipped with a high resolution (Millenium 120) multi-leaf collimator. As the name suggests the MLC consists of 120 leaves collimating the radiation to the shape of the tumor. The 20 leaf pairs at the center have a width of 5mm and the outer 40 have a width of 10mm. The leaves can move continuously with an accuracy of 0.1mm.
For our investigations the possible sources of uncertainties are important coming from the MLC causing low dose radiation due to leakage created by the gaps between neighboring leaves. It is 1.5%-3.5% between the leaves and 12-28% through a closed leaf pair.
The majority of modern linear accelerators are equipped with electronic portal imaging devices (EPIDs). They are used to image and check the patient's position before delivering each fraction minimizing the positional uncertainty. However they might introduce a different one. Since the EPID is retractable and adjustable in its position with Varian LINACS, a small error in its positioning will lead to increased uncertainties during the treatment delivery. This plays a very important role when an EPID is being used for in-vivo dosimetry. Small deviations on the vertical axis lead to a different dose response. The decrease can be described by the inverse-square law (Khan (2009)).

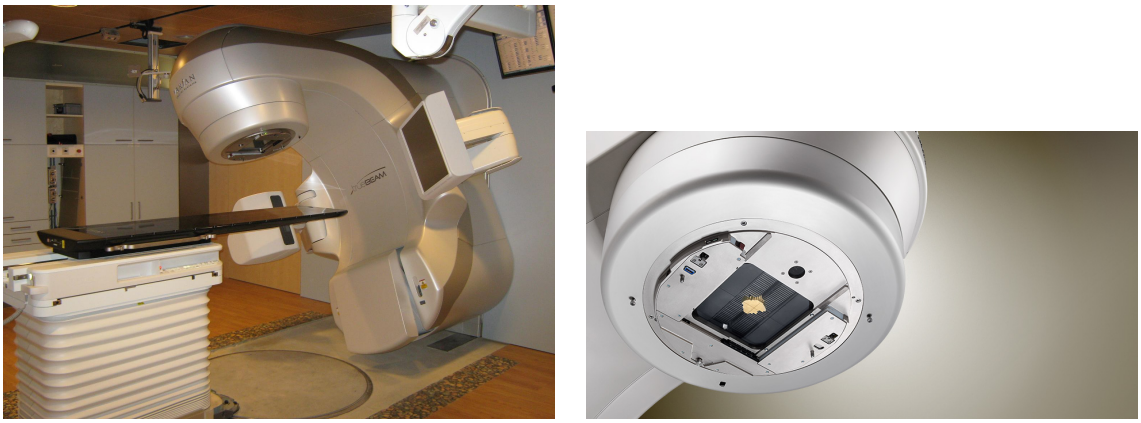

(a) (b)

Figure 4.1: *The c-arm linear accelerator TrueBeam (a) and its 120 millenium MLC (b). In the lower part of the first image you can see the retractable EPID.*

4.1.2 Extraction of the necessary plan data

As described above a lot of different parameters are combined to produce the desired dose distribution. Some of them do not even share the same physical dimension. It is crucial thus to conceive an index to classify and quantify the magnitude of the plan's modulation. This will constitute a basis of comparability among the investigated plans. It is important as well to study the modulation from multiple perspectives: statstics, geometrical, dosimetrical, and a combination of all of them.
The detailed plan components are to be extracted to estimate the modulation of a plan. In a modern TPS, Eclipse by Varian in our case, this treatment information is stored in a unified data format called DICOM, which includes the demographics of a patient, the positioning information as well as the technical plan data like gantry angle, the MLC leaf position etc.
In the case of VMAT plan files the information is split up in so called control points (CP) which are usually placed every two degrees of the arc leading to a total number of 178 CPs for a complete arc of 360°. An automated algorithm was created in Matlab®to open the exported plan file and extract all information affected by the modulation per control point:

- Gantry angle (θ_G)
- Cumulative meterset weight (CMW) (fraction of the dose applied between two adjacent CPs stored as a decimal number between 0 and 1)
- Total dose per arc in Gy

- Total number of Monitor Units (MU) per arc
- Leaf positions of the MLC in mm

The missing factors can now be easily derived:

- Travel distance for each of the 120 MLC leaves by subtracting the positions of adjacent CPs:

$$d_{x,travel} = Position_{x,CP_{i+1}} - Position_{x,CP_i} \tag{4.1}$$

  with x the number of the leaf and i the number of the CP

- Gantry speed ($\overrightarrow{v}_G$). This value is neither stored, nor can it be calculated with the provided information. Nevertheless, in our center the TPS, Eclipse by Varian Medical Systems, was configured according to the manufacturer's guidelines to provide a gantry speed of 4.8°/s as long as being achievable from a mechanical and dosimetrical point of view. This gantry speed is the standard for all clinical plans at our center. The gantry speed per CP can thus be simply and quickly checked before exporting the DICOM file. So far no deviations from the maximum value could be observed.

- Dose delivered between two adjacent CPs:

$$D = (CMW_{CP_{i+1}} - CMW_{CP_i}) \cdot \textit{total dose per arc} \tag{4.2}$$

- Dose rate (DR) of each CP in MU/minute:

$$DR = \frac{(CMW_{CP_{i+1}} - CMW_{CP_i}) \cdot \textit{total number of MU per arc}}{\theta_{G,i+1} - \theta_{G,i}} \cdot \overrightarrow{v}_G \cdot 60 \tag{4.3}$$

  A verification of the values can again quickly be done with the TPS and showed that the calculated numbers match the original ones by 99% or better.

Different factors influencing the modulation as well as combinations of factors were tested in order to establish the sources of the observed deviations. Several indexes have been previously defined, e.g. by McNiven et al. (2010),Webb (2003) or Masi (2013), to characterize and quantify the modulation of a plan. Additional indexes have been conceived for the purpose of this study.

For each definition, the correlation between the modulation index and the results of the DQAs of 121 prostate patients treated by two complete arcs was analyzed. The DQAs were performed on a IBA MatriXX® 2D ionization chamber array. The analyses of the

measurements were done with the commercial software OmniPro I'mRT (IBA). In order to rule out a systematic error of the LINAC, two patient groups treated at different accelerators were included in the investigation. These LINACs were a TrueBeam (Varian) and a 2100C/S (Varian). The results of the DQA were investigated in two manners: as a binary result - passing/failing the 4%/3mm gamma criterion - or in the form of the actual gamma passing rate.
A test plan was created with Matlab to verify the written algorithms. This plan consists of a cylindrical dose distribution within a cylindric homogeneous phantom by setting the MLC leaves to a fixed position of +2.5cm and -2.5cm in the isocenter plane. As such no parameter contributing to the modulation should change, i.e. constant gantry speed, constant dose rate etc. The studied modulation factors are being discussed in the following sections.

4.1.3 Definitions of Modulation Factors

4.1.3.1 Standard Deviation of the Dose Rate

In the case of the VMAT as carried out by Varian Medical Systems, the dose rate varies from CP to CP, regulating the amount of radiation applied within a certain gantry angle interval to fulfill the planning requirements. A vastly changing dose rate might be a good indicator that the plan is too modulated for real conditions. In order to evaluate the influence of the dose rate variability on the performance of the plan, the standard deviation of the dose rate was determined for each arc.

$$\sigma_{DR} = \sqrt{Var(DR)} \tag{4.4}$$

If $\sigma_{DR} = 0$, the dose rate remained unchanged, thus unmodulated, the machine output is a constant number. The higher the standard deviation is the more changes are present, i.e. the higher the modulation.
The values were confronted to the DQA results, both in binary form and the passing rate, as shown in figure 4.2.

4.1.3.2 Adaptation of the Definition used with TomoTherapy

The next factor characterizing the modulation was adapted from a definition used for TomoTherapy units. In TomoTherapy, a modulation index is defined by the maximum leaf open time divided by the average leaf open time. This definition is, in the case of

c-arm LINACs, purely geometrical and is calculated per arc. Since the MLC leaves are not binary as in TomoTherapy units, the definition had to be modified. In analogy to the leaves being open for a certain time, the maximum irradiated surface of all CPs within an arc was divided by the average size of the irradiated area of the corresponding arc.

$$MF_{tomo} = \frac{A_{max}}{A_{average}}|_{arc} \tag{4.5}$$

where A is the irradiated area.

4.1.3.3 Travel distance of the leaves of the MLC

a) averaged over the whole arc

One of the weakest points in the modulation of a plan is the performance of the leaves. Indeed in the case of the sliding window technique, the position of the leaves has to rapidly adapt to the requirements at the next CP. The leaves might therefore need to mechanically drive fast to a new position with a maximum speed of 3cm/s (Arno et al. (2005)). Although the optimization algorithm is set up to minimize the necessary travel distance, extreme scenarios implying extreme modulation levels may require to break a certain limit. Thus, a new factor was defined to establish the influence of the travel distance of one leaf between two adjacent CPs of the arc, since the MLC has 120 leaves and one complete arc 178 CPs, the average and maximum travel distance was taken from all CPs in one arc:

$$MF_{travel,arc} = \frac{d_{travel,max}}{d_{travel,average}} \tag{4.6}$$

b) averaged over the CPs

In order to verify whether an important movement was overlooked by averaging over the complete arc, the definition in 4.1.3.3 was applied to each CP and then averaged over all CPs of one arc:

$$MF_{travel,CP} = \overline{\frac{d_{travel,max,CP}}{d_{travel,average,CP}}} \tag{4.7}$$

4.1.3.4 Adaptation of a definition introduced by S. Webb

Supposing that a combination of several characteristic parameters may play an important role in the modulation, complex definitions of modulation considered, which integrate these parameters into one single modulation index.
An initial complex modulation index was defined by Webb (2003) for IMRT.

In IMRT each beam is subdivided into infinitesimal small pieces called bixels (beam elements in analogy pixels). Each bixel has a different intensity composed of numerous segments. Webb suggested to analyze a beam with n numbers of elements with the bixel intensity I_p with p=1,2,...,n.
The principal idea is to calculate the integral of the spectrum $z_{(f)}$ of the number of adjacent element changes that exceed a certain fraction of the standard deviation of the beam. Thus the standard deviation σ_I of the intensity and the dimension of changes between two neighboring bixels $\Delta_p = |I_p - I_{p-1}|$ are to be calculated.

Next, the number of changes larger than a certain fraction of the standard deviation $[N_{f,\Delta_p>f\cdot\sigma_I}]$ is calculated with f=0.01, 0.02,...2. Thus the spectrum is

$$z_{(f)} = \left(\frac{1}{n-1} \cdot N_{f,\Delta_p>f\cdot\sigma_I}\right) \tag{4.8}$$

leading to

$$MF_{Webb} = \int_0^{0.5\sigma} z_{(f')}\ df' \tag{4.9}$$

Like mentioned above, equation 4.9 was initially designed for IMRT. The bixel intensity I_p has to be slightly adjusted to adapt the definition for VMAT plans. Every control point in one arc is interpreted as a beam and the programmed field size/ shape is one "giant" bixel, thus $I_p \widehat{=} I_{CP}$.

4.1.3.5 Definition adapted by L. Masi

A modulation quantification created by McNiven et al. (2010) for IMRT plans was adapted by Masi (2013) for VMAT plans. This factor is called the "Modulation Complexity Score" (MCS). Its advantage is the combination of leaf mechanical, geometrical, and dosimetrical data. As above, in section 4.1.3.4, the adaption was done by interpreting the control points as an IMRT segment.
The leaf travel information is taken into account by the Leaf Sequence Variability (LSV). The LSV is based on the difference in position of neighboring leaves relatively to the maximum possible difference within each CP per leaf bank:

$$pos_{max,CP} = [max(pos_{n\in N}) - min(pos_{n\in N})]_{leafbank} \tag{4.10}$$

$$LSV_{CP} = \left(\frac{\sum_{n=1}^{N-1}(pos_{max,CP} - |pos_n - pos_{n+1}|)}{(N-1) \cdot pos_{max,CP}} \right)_{leftleafbank} \cdot \left(\frac{\sum_{n=1}^{N-1}(pos_{max,CP} - |pos_n - pos_{n+1}|)}{(N-1) \cdot pos_{max,CP}} \right)_{rightleafbank} \tag{4.11}$$

with N being the number of moving leaves and pos the position of leave n. The LSV is 1 if the leaves do not move during the application of the plan. The more complex a field shape is, with bigger changes in the positional change of neighboring leaves between two CPs, the smaller is this factor.
Next, the complexity of the change of the field shape is included by calculating the Aperture Area Variability (AAV). The AAV is the area between two opposing leaves normalized to the maximum area of the leaf pair of the complete arc:

$$AAV_{CP} = \frac{\sum_{a=1}^{A}(pos_{a,leftleafbank} - pos_{a,rightleafbank})}{\sum_{a=1}^{A}(max(pos_a)_{leftleafbank \in arc} - max(pos_a)_{leftrightbank \in arc})} \tag{4.12}$$

where A is the number of leaves in the arc. The AAV describes the area of the irradiated surface of a given control point in the context of all the surfaces defined by the leaves. Thus, for a square field this value will equal 1. The more the area is different from the maximum area, the smaller the AAV.

The MCS considers that, in VMAT, radiation is applied during the movement of the accelerator. Hence, the average values of two adjacent CPs needs to be calculated and be weighted by the number of MUs delivered between these two CPs:

$$MCS_{arc} = \sum_{i=1}^{I-1} \left[\frac{(AAV_{CP_i} + AAV_{CP_{i+1}})}{2} \cdot \frac{(LSV_{CP_i} + LSV_{CP_{i+1}})}{2} \cdot \frac{MU_{i,i+1}}{MU_{arc}} \right] \tag{4.13}$$

Where I is the number of CPs and $MU_{i,i+1}$ the number of MU delivered between two adjacent CPs. The smaller the MCS, the higher the modulation.

4.2 Results

4.2.1 Standard deviation of the dose rate

No obvious correlation could be observed between the standard deviation of the dose rate and the failing DQAs. The failing and the passing plans present a similar level of dose rate

variability and some plans with very high variations of the standard deviation still pass.

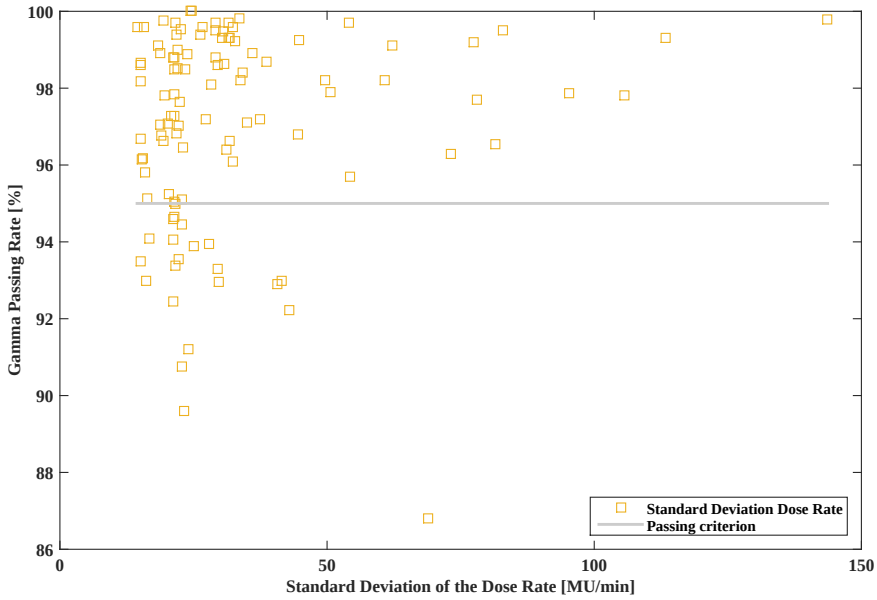

(a) Standard deviation of the dose rate vs. the DQA passing rate. Shown are the MFs of the plan.

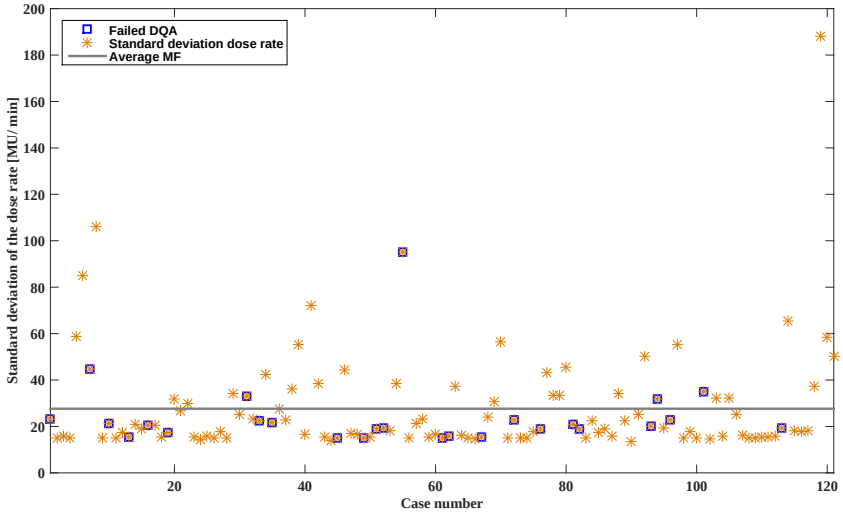

(b) Investigation of the standard deviation of the dose rate in relation to the binary DQA results.

Figure 4.2: *Results of the standard deviation of the dose rate in relation to the actual (a) and binary DQA measurements (b).The red squares in (b) depict the measurements not passing the gamma criterion. Shown are the MFs of the plan.*

4.2.2 Adaptation of the definition used with TomoTherapy

As in the previous section, the modulation factor was confronted to both the binary DQA results and the actual gamma passing rates (see figures X and Y). No direct correlation can be established between the failing DQAs and the magnitude of the modulation of field sizes.

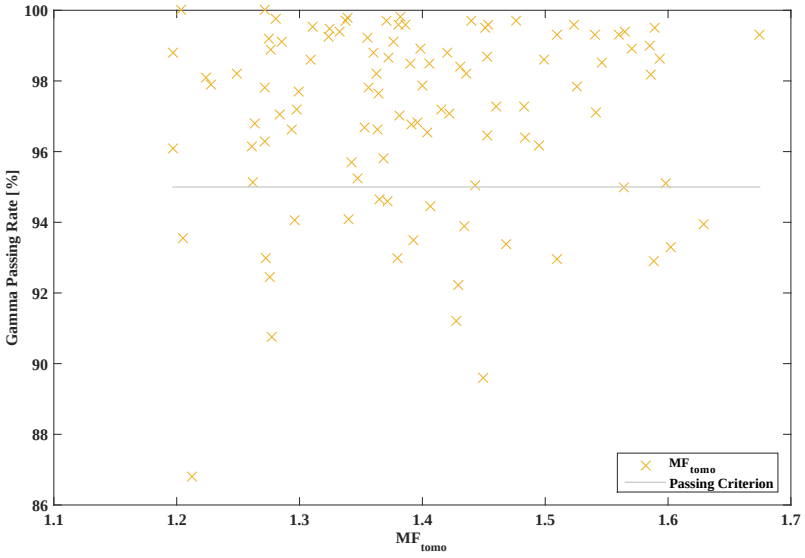

(a) MF_{tomo} versus the gamma passing rate.

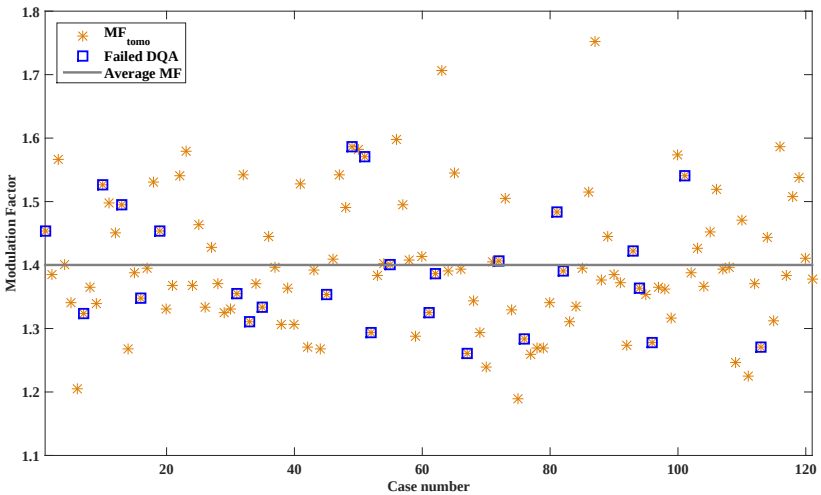

(b) MF_{tomo} binary DQA results

Figure 4.3: *Adaptation of the Modulation Factor as used in TomoTherapy on the actual passing rates (a) and the binary DQA results(b). The red squares show the failed DQA data points of the binary results.*

4.2.3 Travel Distance of the Leaves of the MLC

a) ... Averaged Over the Whole Arc

A comparison to the DQA results in binary form and as gamma passing rates leads to the observation (figure 4.4) that the failing plans have the same magnitude of modulation as the passing ones. As before, even the results with the highest modulation are passing the selected gamma criterion.

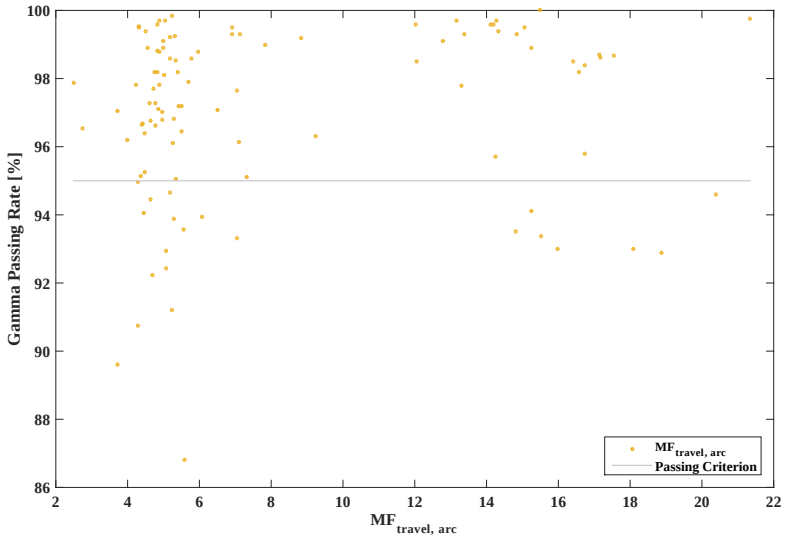

(a) Leaf travel distance averaged over the arc versus the gamma passing rates.

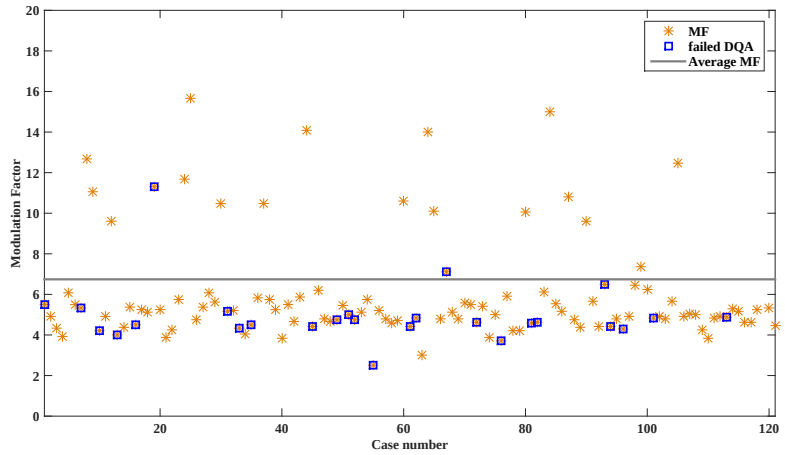

(b) Binary results of the leaf travel distance averaged over the arc

Figure 4.4: *Results of the gamma passing rates (a) of the DQA measurements versus the travel distance between adjacent CPs averaged over the full arc and the corresponding binary results (b). The red squares in (b) mark the failing DQAs.*

b)... Averaged over the CPs

The results of the comparison to the DQAs confirm the previous comparisons by showing (ct. figure 4.5) that failing and passing plans have the same magnitude of modulation.

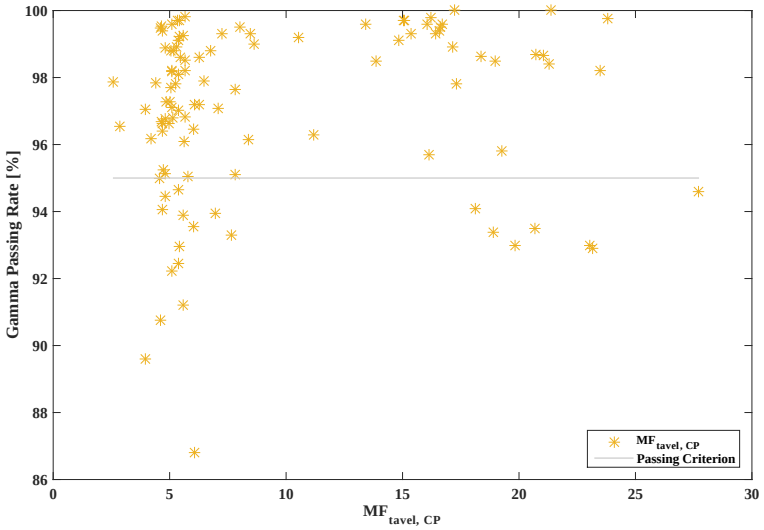

(a) Leaf travel distance averaged over CPs versus the passing rates.

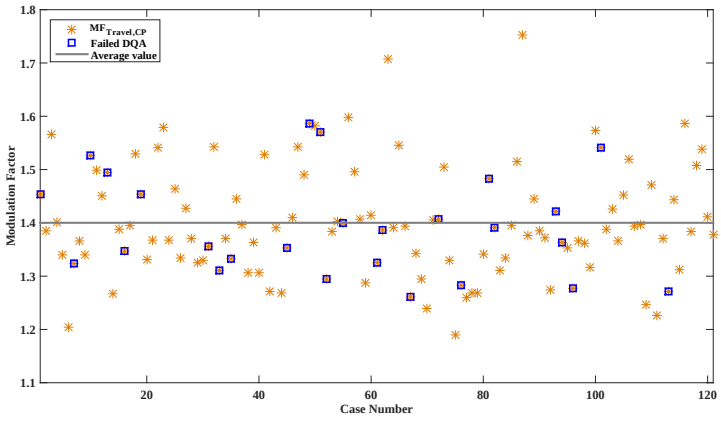

(b) Leaf travel distance averaged over CPs with the binary DQA results.

Figure 4.5: *Results of the gamma passing rates of the DQA measurements versus the travel distance between adjacent CPs averaged over the CPs (a) and the binary results (b). The red squares symbolize the failed DQAs.*

4.2.4 Adaptation of a definition introduced by S. Webb

A comparison against the DQA passing/failing plans (ct. figure 4.6) reiterates the previous results: the plans in the passing and in the failing groups have similar modulations as defined by this modulation factor.

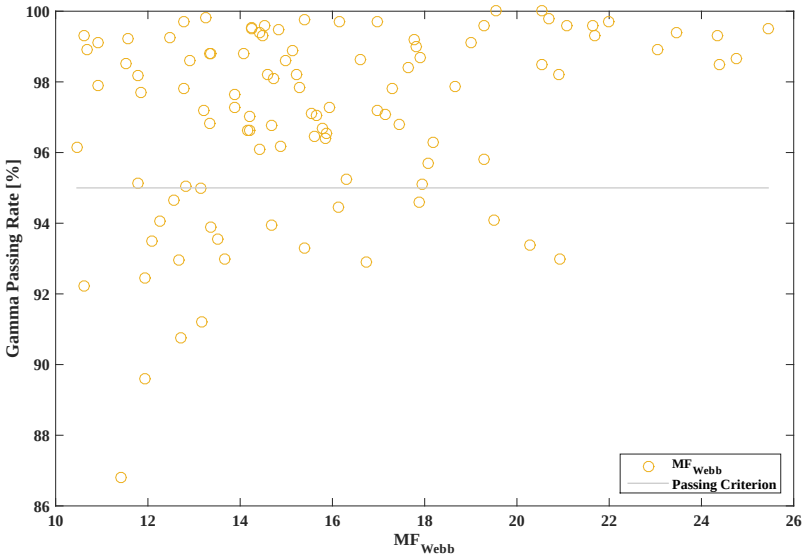

(a) Adaptation of Webb's definition versus the gamma passing rate

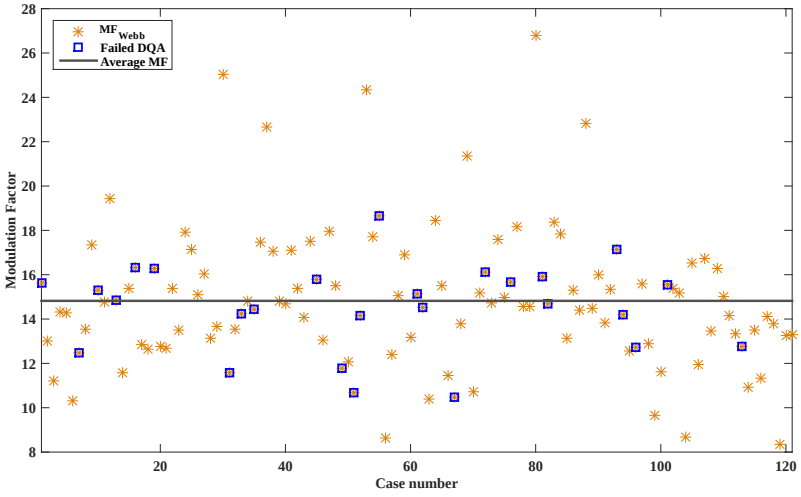

(b) Adaptation of Webb's definition with the binary DQA results

Figure 4.6: *Results of the gamma passing rates of the DQA measurements versus the adaptation of the definition given by Webb (2003) (a) and the binary results (b). The red boxes represent the failed quality checks.*

4.2.5 Definition adapted by L. Masi

Concluding from figure 4.7, there is no clear threshold applying Masi's adaptation of the MCS. Most of the failing DQA measurements are again in the modulation range as the major DQAs passing the gamma criterion. In the published paper one could see a slight tendency between lower MCS, i.e. higher modulation, and lower passing rates. Since the created algorithm was verified using the test plan file where neither leaf motion nor change in the dose rate is necessary the remaining difference is that the publication investigated single arc plans. These require increased modulation, since they need to create the desired dose distribution in only one rotation. Furthermore, the deducted conclusions rely on VMAT plans of various treatment localizations which are not marked in the final results.

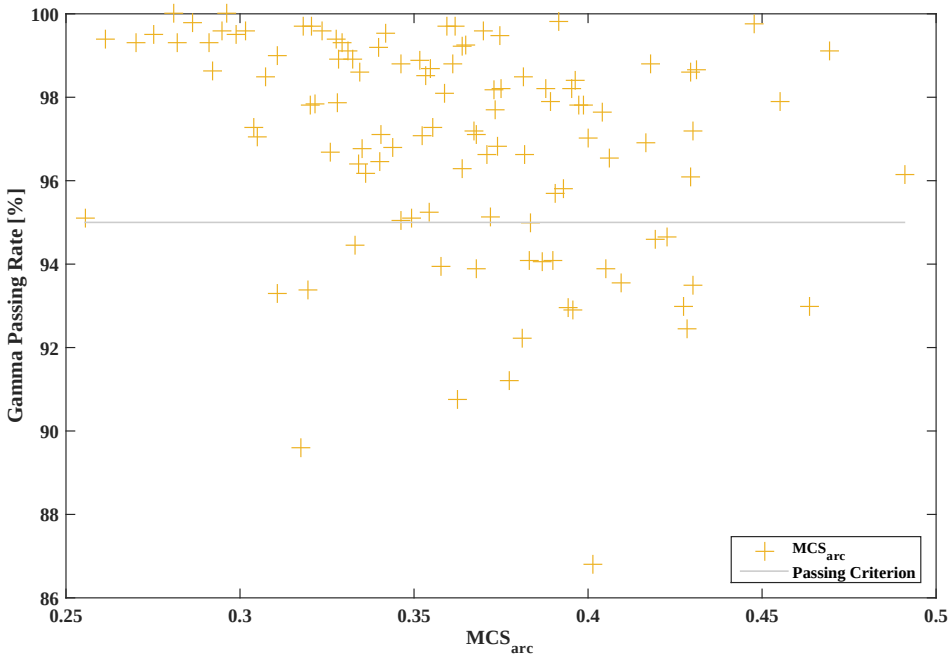

Figure 4.7: *Results of the gamma rates of the DQA measurements versus the definition given by Masi (2013).*

4.2.6 Unbalanced dosimetric distribution between the two arcs

Since no investigated modulation factor showed a clear correlation with the failure of the DQAs, it was decided to pick one reference case and conduct a more detailed study. This case failed the DQA and no reasonable explanation could be found. A simple re-optimization was done, i.e. no parameters were changed. The newly calculated plan passed the DQA without any issues. None of the definitions above showed a considerable

difference. Comparing the two plans's characteristics, it was found that the re-optimizing improved the dosimetric distribution between the two arcs, i.e. both arcs were meant to deliver equally around 50% of the prescribed MUs. Before the re-calculation the first arc delivered 7.87% more of the planned MUs and the second arc just filled the missing dose for completion of the plan with slightly higher modulation factors (ct. table 4.1). In a quick check, several other unbalanced treatment plans were found that did not pass the gamma criterion as well, but there were a few balanced plans that also did not pass. Therefore, this as well seems not be a valid excluding criterion. It might prove to be a fruitful starting point for another through examination in the future.

Table 4.1: *Comparison of the differences between the first and the second arc for the original plan, which failed the DQA and the re-optimized one passing it.*

	Original [%]	Re-Optimized [%]
Total MU	**7.87**	**0.81**
Total Gy	-7.00	7.16
StdDev DR	**48.19**	**1.34**
MF_{Tomo}	-8.13	-1.08
$MF_{Travel,arc}$	3.13	8.57
$MF_{Travel,CP}$	4.38	11.11
MF_{Webb}	-7.08	-4.91
MCS_{arc}	2.40	5.92

4.3 Summary and conclusion

The topic of modulation in external beam radiotherapy is not a trivial problem. Modern techniques provide numerous degrees of freedom to achieve the desired dose distribution, which makes it difficult to combine them to one single parameter. Multiple institutions are currently working on the issue with inconclusive results. The presented work showed that there is neither a clear correlation nor a threshold value for prostate cases treated with dual arc VMAT plans between the magnitude of the modulation and the DQA result as represented by the indexes studied here.

A reason for this could be that prostate cases are generally speaking rather low modulated; this is confirmed by the obtained results. Including other, more complex treatment sites - e.g. head and neck - might show certain tendencies. Additionally, an adaptation of the action level triggered by the gamma passing rate might be a good idea. The task group report 119 of the American Association of Physicists in Medicine (Ezzell et al. (2009)) is recommending to reduce the passing rate down to 90% for a treatment stop based on their

results for small field IMRT measurements with ionization chambers applying a criterion of 3%/3mm. Furthermore, our study was of retrospective nature based on the measured DQA and the theoretical plan data. It is possible that something unforeseen happened during the DQA delivery, which forced the treatment control console to adapt at least one characteristic parameter of the modulation, e.g. reduce the gantry speed, and thusly creating a complete new scenario.
It could be beneficial to normalize the modulation factors, e.g. by their total prescribed dose, to get a more independent basis for comparisons. Further work in the future is to consider more statistics, i.e. creating a bigger sample size and database of numerous treatment sites. One should also study the effect mentioned in the last section. It seems that the way of the optimization plays a role in the modulation by influencing the dosimetric distribution on the arcs.

While writing this thesis, a new article was published presenting an approach of phantomless IMRT DQA (Valdes et al. (2016)). It is a theoretical calculation considering 78 uncertainties of metrics that might influence the DQA result. The most influential factors are:

1. Amount of MUs per Gy
2. Number of small apertures
3. Aperture irregularity
4. the fraction of beams delivered outside circles of specific radii

These results confirm our findings that dosimetric and geometric data of the beam needs to be investigated. Instead of the performance of the leaves it seems to be more important to consider the actual beam shape and its irregularities.

Chapter 5

Uncertainties in TomoTherapy

In comparison to conventional linear accelerators the TomoTherapy units are rather new. Their advanced features are very similar to the approach of VMAT: The accelerator is rotating around the patient while applying the planned irradiation. With the introduction of the helical TomoTherapy another degree of freedom was created, since - in addition to the accelerator - the treatment couch moves as well.
The new factor setting the two movements in correlation is called pitch and indicates the distance the treatment couch traveled in one gantry period. At the time of the introduction of TomoTherapy it was new as well that the treatment couch itself was able to correct rotational displacements of the patient in relation to the planning kVCT. Already knowing about the complexity of moving leaves in combination with a moving accelerator, one can imagine the new level of modulation by adding a moving and rotating patient.
Due to the CT-like structure of a TomoTherapy unit only a small number of studies were done using film dosimeters, diodes or 2D arrays replacing the patient to investigate the uncertainties occurring in TomoTherapy treatment deliveries. However, we still depend on unknown factors in real treatment conditions:

"We plan, do the DQA, and send the patient in, hoping for the best, knowing that undetermined uncertainties are occurring" - A medical physicist and former TomoTherapy employee

In-vivo dosimetry (IVD) is a possible approach to find out what happens during a treatment delivery. IVD applies a detector of choice measuring the dose while the patient is treated. On the one hand the clinical staff can detect errors, both statistic and systematic, of each fraction and on the other hand they can use the IVD system to evaluate and check

the used machine and the treatment chain in general.
In cooperation with 21st Century Oncology (Madison, Wisconsin, USA), two software applications were developed to recover and examine all relevant data of the actual treatment delivery. These tools were introduced into the clinical routine for both TomoTherapy units at the Institut Curie as well as tested in real clinical conditions over 18 months in the case of "TomoGamma" and 4 months in the case of "TomoAdaptive".
Thanks to the results obtained with these applications, we conduct in chapter 5.6 a first comprehensive study on uncertainties in TomoTherapy by analyzing the results of transit in-vivo dosimetry and machine data of actual clinical cases. Furthermore, it is presented how the tools can be used in daily clinical routine as a first approach towards adaptive radiotherapy.

5.1 Materials & Methods

5.1.1 TomoTherapy

The experiments related to this chapter were done using two TomoTherapy®Hi·Art accelerators. TomoTherapy units were developed as a CT-Scanner-like machine with an embedded acceleration line that can provide energies used in regular radiotherapy. The linear accelerator is underneath a closed housing rotating around the treatment couch (ct. fig. 5.3) allowing following treatment modes:

- TomoDirect^{TM}, where the accelerator is set to a fix angle and does not move while the radiation is applied. It is equivalent to step'n'shoot IMRT in terms of the low level of modulation.

- TomoHelical^{TM}. Here, the gantry rotates and applies radiation to the patient, who is lying on a moving treatment couch. Due to the capability of creating high modulated plans, this modality can be compared to VMAT.

The accelerators at the Institut Curie produce photons of a nominal energy of 6 MeV at a nominal dose rate of 850 MU/min (System (2011)). The energetic output of the gantry is measured, amongst others, by three transmission ionization chambers placed between the patient and the accelerator. They are hermetically sealed dual chambers with a precision and linearity of 1% each. They can trigger beam-off safety protocols by monitoring, e.g. the dose. Hereafter, these detectors will be called the "head detectors". It is worthwhile mentioning that these chambers are not being used to control the duration of a treatment

delivery. In conventional LINACs the length of a fraction is determined by the amount of dose being measured by the on-board system. This approach is necessary, since with this type of accelerators the energy and dose rate can change from plan to plan. With TomoTherapy these two factors are meant to be constant and the duration of a treatment is thus defined by the integration of time. Therefore, the consideration of uncertainties is also different.
Normally, the data specifying a treatment plan is saved in DICOM format, where they can be accessed by e.g. control points as mentioned above. However, in the case of TomoTherapy the data is stored differently. Since the accelerator rotates several times around the patient it is too difficult to distinguish the multiple gantry positions of the same angle. Instead the system provides what is called a plan sinogram. The rotation leads to numerous (several hundreds or even thousands depending on the irradiated volume), so called, dose projections from different angles creating a sinus shaped curve if plotted together (ct. figure 5.1). In a plan sinogram the leaf number is shown against the dose projection number. The color scale is giving the time that a leaf is open in seconds, which is, due to the constant energy and dose rate, a direct indicator of the dose. As such the sinogram is the equivalent of a 3D dose map in space and time.

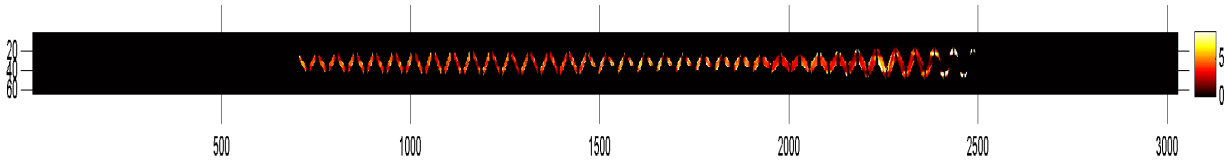

Figure 5.1: *Example of a plan sinogram from an actual spine case. One can see sinus shape of the curve. In the 3D plot the x-axis is the dose projection number (in total more than 3000), the y-axis the leaf number of the MLC and the color indicates how many seconds a leaf was open.*

One of the unique characteristics of the Tomo units is the capability of reconstructing a full CT with energies in the range of MeVs, thus called MVCT, verifying the patient's position referring to the planning kVCT prior to the beginning of a treatment. This MVCT is recorded by a special designed arc-shaped detector rotating with and always opposing the linear accelerator. With the development of the TomoTherapy machines the detectors changed as well leading to different detector models available for a unit (ct. table 5.1). Their advantages in comparison to EPIDs are their fixed positions, thus eliminating the positional uncertainty of the detector. Since the detector has a different curvature than the bore of the Tomo unit, it is important to consider the different structure, because the obtained signal needs to be corrected to achieve the actual beam profile.

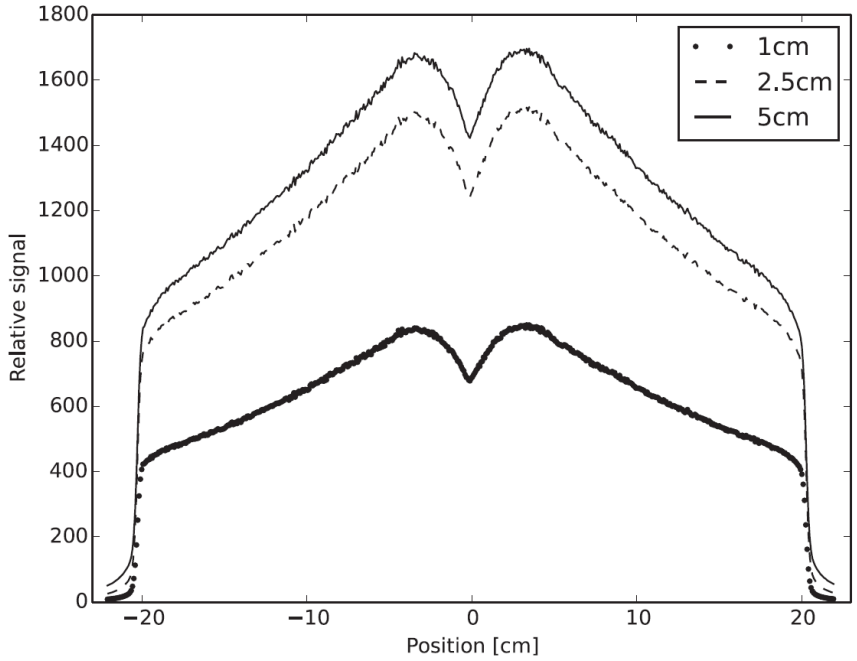

Figure 5.2: *The uncorrected signal of the arc detector measuring the profiles of the three possible open fields in TomoTherapy. Due to the different curvature of the detector than the LINAC rail a dip occurs for the center channels, which is amplified by the non.coplanar fan beam.©Pisaturo et al. (2015)*

Table 5.1: *Several generations of detectors are available having different characteristics as shown below. The detector used for this thesis was of the third generation (bold text and framed).*

	Detector 1	Detector 2	**Detector 3**	Detector 4
width of detector element [cm]	0.1219	0.118	**0.12503**	0.1242
radius of curvature [cm]	110.99	98.6	**99.8**	139.6
detectorSurfaceToAxisDistance [cm]	56.95	47.3	**57.2**	54.6
detectorSurfaceToCenterDistance [cm]	2	0	**0.4**	0
lowChannelOpenField	56	60	**26**	30
HighChannelOpenField	595	579	**553**	549

The only common point between all detectors is that each detector arc is consisting of certain number of Xenon-gas filled chamber divided into several chambers by septal plates. The used units were equipped with the detector given in the third column.

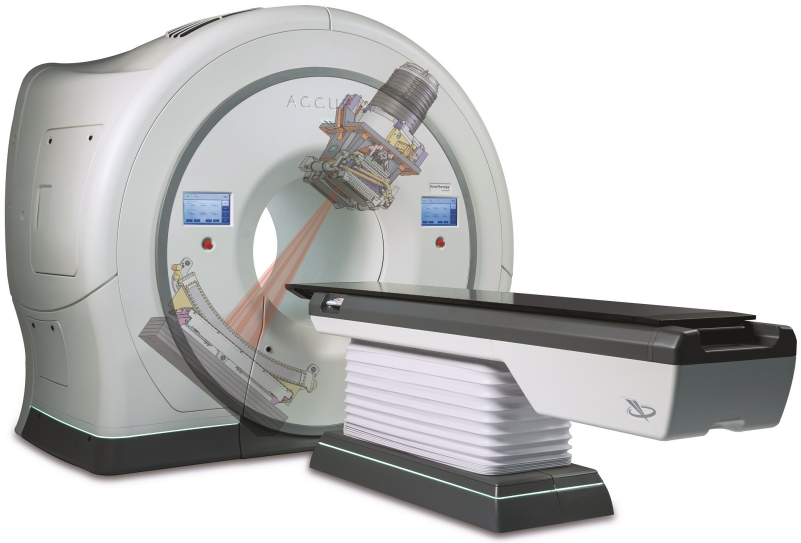

Figure 5.3: *Image of a Tomotherapy unit indicating the rotating linear accelerator underneath the housing. And the opposing detector arc. ©Accuray Inc.*

Another advantage, especially from a scientific perspective, is that all treatment information is stored in a log file in XML format that is automatically created when archiving the patient. All major patient and machine data are stored in it, such as the machine output, gantry speed, patient setup, patient setup corrections etc. Even more information can be downloaded directly after each treatment from the system by a ftp connection as a CSV-file, e.g. gantry angle per projection, chamber signal per projection, cooling water temperature..

Another unique fact in comparison to LINACs is the binary MLC. Binary already indicates that each leaf can have only two states: open or closed. They are driven by hydraulic forces using air pressure. Available field sizes are 1cm, 2.5cm, and 5cm for each of the 64 leaves. Since the binary mode restricts the capability of modulation, a new modality called TomoEdge^{TM}was developed. It is not included in this work, as it was not available in our clinic.

The used software version controlling the Tomo units and planning was version 5 (build: 5.0.2.26, planning station 5.0.2.5).

5.2 System description of "TomoGamma" and "TomoAdaptive"

5.2.1 "TomoGamma"

The first of the two programs is called "TomoGamma". Its aim is to check all the technical aspects of a treatment such as machine output, patient positioning, comparison between reference kVCT, and actual MVCT.
The data is collected by the detectors built into a TomoTherapy unit: three overhead ionization chambers for the dosimetric output and the MVCT imaging detector facing the LINAC. Furthermore, the TomoSystem itself records machine data: among others, the gantry angle of each dose projection, the adjustment of patient positioning prior to the treatment. All these data are stored in the patient archive, which can be retrieved at any time via a ftp connection.
The archive is imported into a directory constantly scanned by "TomoGamma" to initiate all the necessary calculations as soon as a new archive is available. For example a gamma analysis for each projection transforming the analyses to a 3D gamma passing rate, making it possible to locate the point of failure within the patient's CT to analyze if a certain local anatomical structure or change is responsible for a low gamma passing rate. This detection is already the first step of adaptive radiotherapy, because it is detecting the influence of anatomical changes that require a re-planning fraction by fraction.
The passing rate is created by calculating the differences between the analyzed treatment fraction and a reference fraction, which is by default the first one but can be changed to any available fraction of the plan. The passing rate is calculated for each of the dose projections, usually 51 per rotation, and then averaged over all projections. The results are available in coronal, sagittal, and rotational perspective.
The gamma value calculation is based on the pixel values of the projection's image registered by the imaging MVCT detector. These values do not contain direct dosimetric information; hence, an comparison of absolute dose, e.g. to the plan, is currently not possible.
Only a relative gamma comparison of two fractions is available at this point, as the calculations are based on the pixel values of the projection's image recorded by the imaging MVCT detector. These values do not contain direct dosimetric information. The default gamma criterion is set to 3%/3mm and the passing rate to 95% of the pixels having a gamma value ≤ 1, but these values can be changed to any value at any time for all pa-

tients, one single plan, or even for only one fraction.
Based on the measured output, one can determine the dose rate by multiplying the output value with a constant factor proprietary to 21st Century Oncology. The two CTs, planning kVCT and MVCT of a fraction, are merged and superposed in different coloring highlighting any differences to the anatomy and positioning recorded during the reference treatment fraction. Additionally, the two CTs are compared to each other based on pixel intensities. A factor called "Similarity" quantifies any difference between the images ranging from 0 to 1, where 1 is a perfect match of the CTs and 0 indicates that not a single matching pixel could be found.

Table 2.1. Thresholds

Parameter	Value	Comments
translationOffset	[1 2]	cm
rotationOffset	[3 5]	degree
KVMVSimilarity	[0.95 0.9]	
outputMean	[0.015 0.03]	
outputVar	[0.03 0.06]	
gamma	[97.5 95]	%

Table 2.2. Treatment Summary

fraction#	date.time	IGRT	translation	rotation	similarity	outputMean	outputVar	gamma	Comments
1	20130204.142847	IGRT	Green	Green	Green	Green	Yellow	Green	
2	20130205.134742	IGRT	Green	Green	Green	Green	Yellow	Green	
3	20130207.130434	IGRT	Green	Green	Green	Green	Yellow	Green	
4	20130208.175320	IGRT	Green	Green	Green	Yellow	Yellow	Green	
5	20130211.170327	IGRT	Green	Green	Green	Green	Yellow	Green	
6	20130212.184000	IGRT	Green	Green	Green	Green	Yellow	Green	
7	20130213.185708	IGRT	Green	Green	Green	Green	Yellow	Green	
8	20130214.185127	IGRT	Green	Green	Green	Green	Yellow	Green	
9	20130215.181825	IGRT	Green	Green	Green	Green	Yellow	Green	
10	20130218.150634	IGRT	Green	Green	Green	Green	Yellow	Green	
11	20130219.093200	IGRT	Green	Green	Green	Green	Yellow	Green	
12	20130220.180032	IGRT	Green	Green	Green	Green	Yellow	Green	
13	20130221.144743	IGRT	Green	Green	Green	Green	Yellow	Green	
14	20130226.090222	IGRT	Green	Green	Green	Yellow	Yellow	Green	
15	20130227.092028	IGRT	Green	Green	Green	Yellow	Yellow	Yellow	
16	20130228.183940	IGRT	Green	Green	Green	Red	Yellow	Green	
17	20130301.171925	IGRT	Green	Green	Green	Red	Yellow	Green	
18	20130304.140108	IGRT	Green	Green	Green	Red	Yellow	Yellow	
19	20130305.092059	IGRT	Yellow	Green	Green	Red	Yellow	Yellow	
20	20130306.095158	IGRT	Green	Green	Green	Yellow	Yellow	Green	
21	20130307.122635	IGRT	Yellow	Green	Green	Yellow	Yellow	Yellow	
22	20130308.170017	IGRT	Green	Green	Green	Yellow	Yellow	Green	
23	20130311.151505	IGRT	Green	Green	Green	Yellow	Yellow	Green	

Figure 5.4: *Treatment result dashboard of a radiotherapy plan in "TomoGamma". It shows the analyzed parameters, i.e. patient positioning (translation, rotation), anatomical changes by comparing the planning kVCT and daily MVCT (similarity), machine output (outputMean, outputVar), and the global gamma result. The thresholds for each column are given in the table above the results. A deeper analysis of each fraction can be done by selecting on the corresponding link in the second column.*

In the context of clinical routine, a considerable amount of time is spent to analyze the obtained results, even though mostly failing fractions are of interest. Thus, a three-colored based warning system was introduced in the general overview to speed up the evaluation process. It shows the amount of all fractions delivered to the patient and their rated results.

Table 5.2: *Flagging criteria for all calculated factors for analyzing the treatment's quality.*

	Gamma Passing rate [%]	Similarity	Output Variance	Output Mean	Translation Offset [cm]	Rotation Offset [°]
Green	>97.5	>0.95	<0.03	<0.015	<1	<3
Yellow	(97.5,95)	(0.95,0.9)	(0.03,0.06)	(0.015,0.03)	(1,2)	(3,5)
Red	<95	<0.9	>0.06	>0.03	>2	>5

5.2.2 "TomoAdaptive"

Since "TomoGamma" is restricted to technical machine data and allows neither a comparison in absolute dose nor a comparison of the measured results to the planned data; an additional tool was developed with 21st Century Oncology: "TomoAdaptive".
The idea is to use both programs as complementary tools. "TomoGamma" indicates that one or multiple technical factors failed during a treatment and "TomoAdaptive" assesses the clinical impact done from a dosimetrical perspective.
Once again the user only needs to push the patient archive to the incoming folder if he desires to start the adaptive calculation manually. As, at the Institut Curie, we use both applications, it was possible to provide certain automation to the process. The files were exported once to "TomoGamma". As soon as "TomoGamma" is finished with its analyses, the files will be pulled by "TomoAdaptive" automatically to start its calculations. The software then retrieves the necessary information. This includes the planning kVCT, planned sinogram, contoured structures, prescribed dose, planned dose distribution, and the MVCT of each fraction.

"TomoAdaptive"'s aim is to assess the success of a treatment delivery through several data:

- It shows a merged CT of the planning kVCT and the MVCT of the analyzed fraction to detect major anatomical changes.
- Data of the original plan: the kVCT superposed by the planned dose distribution and original ROIs.
- The daily MVCT superposed by the deformed ROIs. The deformation is calculated by using the image intensity based Morphon's algorithm (Latifi et al. (2013), Wrangsjö et al. (2009), Forsberg et al. (2007), Plumat et al. (2009)).

- As additional layer in this view the changed dose distribution is calculated, caused by the change in the anatomy with the help of the extracted plan data. The dose calculation is performed by a collapsed cone convolution-superposition algorithm (Ahnesjö (1989), Oyewale (2013)) and is a complete re-calculation.

These datasets are now utilized to derive even more information for each contoured ROI, which helps to assert the quality of the treatment:

- Received dose based on the deformed information compared to the plan, both for each fraction and cumulative.
- Dose-Volume-Histogramm (DVH), both for each fraction and cumulative.
- Changes in volume of the ROI.
- Position of the ROI's centroid to estimate organ movement.

In order to guarantee a correct analysis, it is important that the investigated structure is sufficiently imaged, at least 95%, during the daily MVCT. It is clear that a DVH, position data, and volume information are incorrect if parts of the volume are - or rather cannot - be considered in the calculation due to missing information.

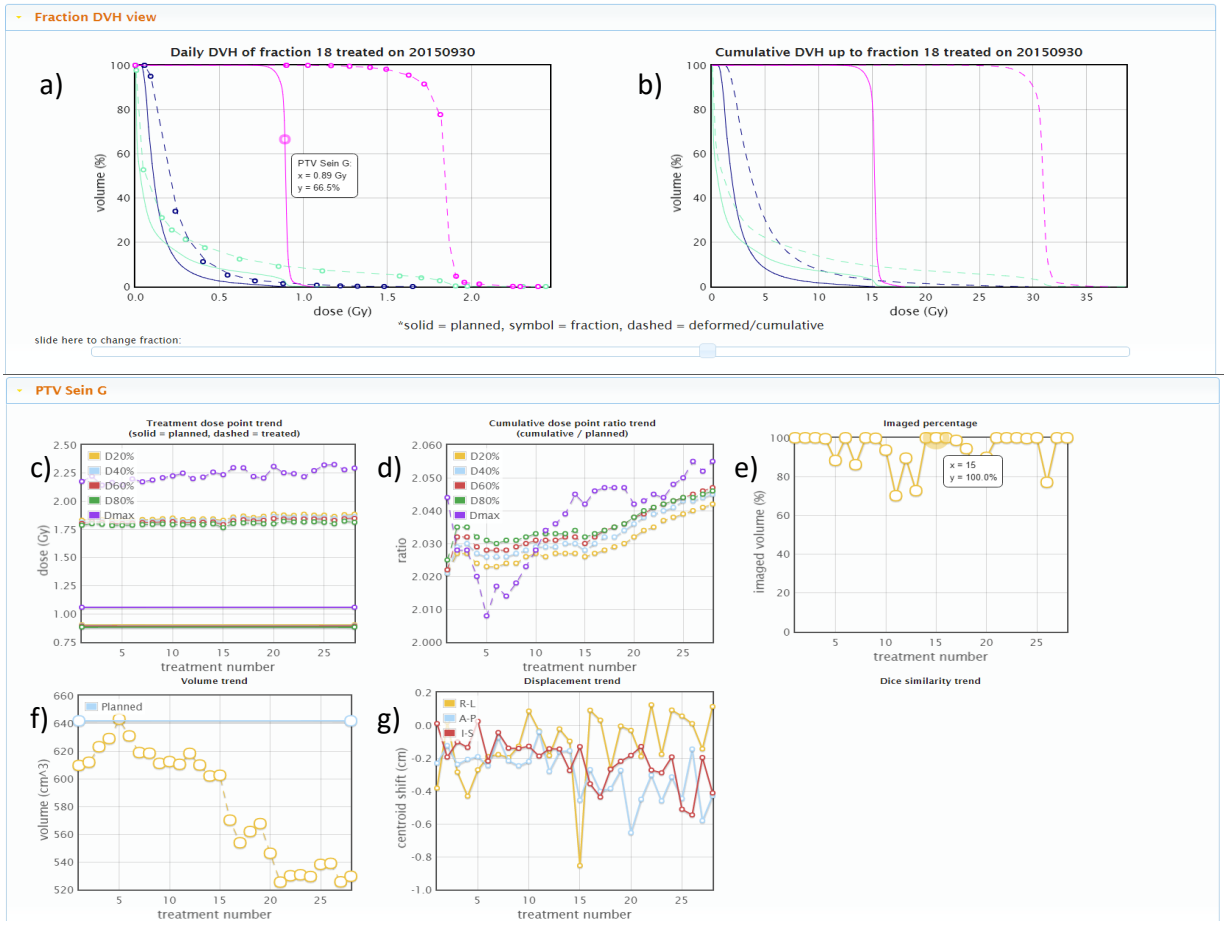

Figure 5.5: *The "TomoAdaptive" dashboard for a breast patient plan. The upper part shows the DVHs of the three selected ROIs (a), and b)). The lower part represents the rest of the information such as volume (f)), displacement (g)) or imaged percentage (e)) for the ROI "PTV Sein G", which is the target volume in the left breast. Additionally, one can change to the comparison of the four CT windows in "Fxs viewer" or "Cumulative viewer".*

In the main window on the top the DVHs are shown. The left one (a)) displaying the result of the selected fraction (here no. 18, selected with the slider below the DVHs). It displays

- The planned DVH (solid line)
- Per fraction results, i.e. of the deformed ROIs and the dose distribution on the MVCT (symbols)
- The DVH based on the deformed ROIs mapped back to the planning CT (dashed line)

The right graph (b)) is depicting the cumulative DVH up to the moment of the selected fraction. Again presenting

- The planned DVHs (solid line)
- The DVHs based on the information of the deformed ROIs mapped back to the planning CT (dashed line)

Down below one can investigate further information:

- Dose trend fraction by fraction (c))
- Cumulative dose trend (d))
- Imaged percentage (e))
- Volume change (f))
- The displacement of the geometrical center of a ROI (g))

Since the data is written in HTML5 it is easy to open and transfer and allows to retrieve data of specific points by hovering the mouse over the graph (ct. figure 5.5 in the graph of "Imaged percentage", where the cursor hovered over the 13th fraction).

5.3 Assessing the sensitivity of "TomoGamma"

Although having an application based on approved and routinely used methods, it is necessary to verify if the information given is correct and has a sufficient sensitivity, especially when they are used in a novel implementation that never was done before. Thus, several tests with different levels of complexity were created to benchmark the software.

Three different phantoms (TomoPhantom, also referred to as the "cheese", the RANDO phantom, and the CIRS Thorax) are being irradiated in helical TomoTherapy. The phantoms themselves pose certain challenges. The Cheese is cylindrical and can be homogeneous or heterogeneous by inserting plugs with different electron densities.
The Rando head is homogeneous but is irregularly formed with proportions of a real human head. The third phantom is heterogeneous and imitates the difficult scenario of a thoracic treatment, e.g. breast cancer. In addition, several changes within the planning are applied: simple cylindrical targets in the center and off center overlapping with the heterogeneities, as well as ring structures around the center. More detailed information on the test geometries will be given in the corresponding sections for a better overview.

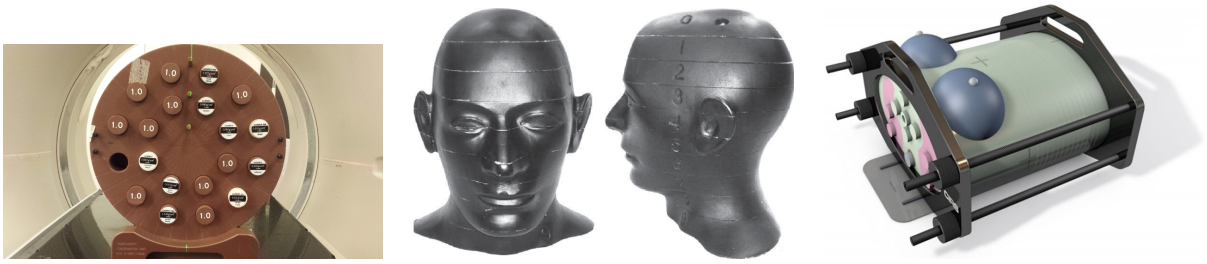

(a) (b) (c)

Figure 5.6: *The three phantoms used to characterize the software's limitations: The "cheese" (a), the RANDO head phantom (b) ©Radiology Support Devices, and the CIRS Thorax (c) ©Supertech.*

For the purpose of testing "TomoGamma", each case will consist of several fractions including the reference, i.e. correct setup and kVCT identical density configuration, and fractions with a changed setup, e.g. shifted in all three dimensions and in rotation.
Furthermore, anatomical variations, i.e. reduction of a bolus from 3cm to 0cm and addition of heterogeneities are introduced from fraction to fraction. The bolus simulates a change in the patient's anatomy.
The dose variation is verified by comparing it to an absolute dose measurement recorded with an ionization chamber A1SL (Standard Imaging). In order to detect even smaller differences a sensitive gamma of 2%/ 2mm is applied and the passing rate is set to 95%.
The created plans for the cheese and the RANDO were calculated to apply a total of 120 Gy in 60 fractions to the target volume. For the CIRS phantom a plan following the in-house standard for breast treatments was created including the present OARs in a breast case, such as the lungs, the heart, the spine, and others. The protocol prescribes 51.8 Gy in 28 fractions to the PTV.
Despite the greatest effort to perfectly recreate the phantom's position in the planning CT, there will always be some minor differences. The results of the dosimetric analysis and the CT comparison are normalized to the values of the reference fraction to account for these deviations.

5.3.1 Results

5.3.1.1 CIRS phantom

The phantom was contoured following the different structures as present in a breast case created by the varying densities within the phantom. It is provided with a drilling to insert an ionization chamber. Several layers of bolus material were laid upon the "breast"

to simulate a loss of volume during the treatment course. The layers have a thickness of 0.5cm and were removed one after the other.

Table 5.3: *The results of the measurements using the CIRS phantom with stepwise bolus reduction. The differences (Δ) are normalized to the reference fraction.*

Bolus reduction [cm]	Measured Dose [cGy]	Passing rate [%]	$\Delta_{passing\ rate}$ [%]	$\Delta_{dose,chamber}$ [%]
0	188.53	99.99	0.00	0.00
0.5	190.33	98.04	1.95	0.96
1	190.33	90.51	9.48	0.96
1.5	193.95	83.97	16.03	2.88
2	196.36	79.74	20.26	4.15

The table above shows that the gamma evaluation is failing at a reduction of the thickness of 1cm by lowering the passing rate by 9.48%, whereas the ionization chamber measured only a difference of less than 3%. Thus, "TomoGamma"'s sensitivity is higher for volume changes in the direction of the beam. Even the reduction of 0.5cm leads already to a decrease of 2% of the passing rate, whereas the mean dose in one point does not measure a significant difference.
Using the obtained results as fixing points for functional fit, it can be concluded that a change 0.7cm will lead to red flagged gamma and already a change >0.5cm will lead to a passing rate lower than 97.5% which is the threshold for the warning level (yellow flag).

5.3.1.2 RANDO phantom

The RANDO phantom was shifted by 10mm and 20mm in all three dimensions. Additionally, a rotational shift of 10° and 20° was tested separately. A comparison with the ionization chamber could not be done, since the phantom has no cavity to insert one.
Additionally the similarity checks of the CTs were analyzed.
The cylindric PTV had a diameter of 2cm and a length of 2cm and was placed above the OAR. An organ at risk of 3cm in diameter and 6cm in length was placed at the center of the phantom.

Table 5.4: *Results of "TomoGamma" with the RANDO phantom applying directional and rotational shifts. In addition to the passing rates the similarity values of the CT comparison were included.*

Shift direction	Shift [mm]	Passing Rate [%]	CT Similarity [%]
Reference	0	99.86	0.98
Transversal	10	96.57	0.91
	20	94.09	0.84
Longitudinal	10	99.71	0.94
	20	97.88	0.88
Vertical	10	97.36	0.91
	20	94.80	0.85
Rotation	10	97.94	0.96
	20	94.95	0.92

With the exception of the shift in longitudinal direction, the directional shifts of 20mm and the rotation of 20° lead to failing gamma passing rates, whereas the shifts of 10mm/ 10° triggered the warning level in the best case or remained undetected by the gamma analysis in the worst case. This is due to the homogeneous nature of the phantom, since there are not a lot of dosimetric differences with smaller shifts when the photons are still attenuated by the same material. Especially moving the phantom in longitudinal direction, i.e. orthogonal to the beam, with a cylindrical phantom will not create a dosimetrical change. The similarity values of the CT signaled a problem by failing their passing criteria of 0.95 at a shift of 10mm.

By creating a curve fit, it was concluded that "TomoGamma"'s sensitivity of directional shifts in transversal direction is 18mm and for rotations it is 19 ° relying only on the gamma passing rate.
The sensitivity increases by 13mm by taking the CT comparisons into account. Thus, shifts larger than 5mm and rotations larger than 13 ° will be flagged with a failure even in homogeneous conditions.

After testing the detection sensitivity of the gamma criterion and the similarity value separately, the following experiments with the cheese phantom will consider these criteria in combination and stepwise change the complexity of the scenario.

5.3.1.3 Cheese phantom with an homogeneous configuration

Centered targets with no OAR

The first plan of the homogeneous setup targets at a PTV volume in the center of the phantom. It has a diameter and length of 3cm each and serves as a GTV. A second target is placed at the center as well and is a cylindrical ring structure around the GTV with an inner diameter of 3cm, an outer diameter of 6cm, and a length of 6cm serving as the PTV. The total dose prescribed to the second target was 108Gy. No OARs were introduced.
This test is the most challenging one for "TomoGamma". The phantom is homogeneous and circular symmetric, such as the target volume. Hence, all beaming directions will be equally weighted and small differences in the position are not expected to have a big impact on the dose distribution.

Table 5.5: *Results of the cheese with homogeneous setup and two centered target volumes.*

Shift direction	Shift [mm]	Measured dose [cGy]	Passing rate [%]	CT Similarity	$\Delta_{passing\ rate}$ [%]	$\Delta_{dose,chamber}$ [%]
Reference	0	203.34	99.92	0.99	0.00	0.00
Transversal	6	205.43	99.62	0.97	0.30	1.03
	15	195.85	99.20	0.94	0.73	3.68
Longitudinal	6	203.04	99.89	0.99	0.03	0.15
	15	200.04	99.82	0.99	0.11	1.62
Vertical	6	201.84	99.66	0.97	0.26	0.74
	15	204.84	99.03	0.94	0.89	0.74

As described above, this is the most challenging setup for "TomoGamma". Therefore, it is no surprise that most of the shifts remained undetected, except for the transversal and vertical shift of 15mm, where the CT similarity started to flag a problem. The ionization chamber measured a difference larger than 2% only for the transversal 15mm shift.
The sensitivity of "TomoGamma" is superior to the point measurement of the ionization chamber. The CT comparison parameter created a warning at a shift of 6mm in both transversal and vertical direction. As concluded from a curve fit based on the results of the similarity factor, shifts bigger than 12mm will be failing the comparison criterion.

Centered PTV with two off-center OARs

The next test with the homogeneous configuration included a PTV at the center of the phantom with a diameter and a length of 6cm each. The two cylindrical OARs had a diameter and length of 6cm as well. Using the phantom's center as origin of a Cartesian

coordinate system the OARs's centers were placed at (5.66cm, 5.66cm) and (-5.66cm, 5.66cm). The objectives for the OARs were a maximal dose of 30Gy for the first one and 40Gy for the second one.

Table 5.6: *Results of the test case with a homogeneous configuration of the phantom. The dose of the centered target had to be achieved by sparing the two off-centered OARs.*

Shift direction	Shift [mm]	Measured dose [cGy]	Passing rate [%]	CT Similarity	$\Delta_{passing\ rate}$ [%]	$\Delta_{dose,chamber}$ [%]
Reference	0	203.34	99.94	0.99	0.00	0.00
Transversal	6	202.15	99.73	0.97	0.21	0.58
	15	200.37	99.53	0.94	0.41	1.46
Longitudinal	6	203.34	99.91	0.99	0.04	0.00
	15	203.34	99.82	0.99	0.13	0.00
Vertical	6	203.93	99.84	0.97	0.10	0.29
	15	203.93	99.61	0.94	0.34	0.29
Rotation	10	203.34	99.88	0.99	0.06	0.00
	20	203.34	99.85	0.99	0.09	0.00

The results show almost the same tendency as before, only the 15mm shifts in transversal and vertical direction created a failing value of the CT similarity comparison. Since there are no changes in the density, a small change in the dose distribution was not expected to create greater errors. The ionization chamber did not even measure a single difference larger than 2%.
Disturbing the equivalent beam weights does not seem to improve the detection threshold. As a next step the symmetry will be broken by moving the PTV out of the center.

Off-centered PTV and centered OAR

As the last test using the homogeneous setup, a PTV was placed at (5.66cm, 5.66cm) with a diameter and length of 4cm each. The centered OAR is the previous used target at the center with a planned objective to not receive more than 30Gy. Since the first experiments did not reveal errors in the gamma analysis it was decided to shift the phantom by 20mm and 25mm in transversal, 20mm and 40mm in longitudinal, and 20mm and 30mm in vertical direction. The rotational difference to the reference fraction was set to 15° and 35°. By doing so, it was expected to obtain at least one data point failing the gamma passing criterion.

Table 5.7: *Results of the cheese phantom having an homogeneous setup. This time the target was shifted to a position with 8cm distance to the phantom's center at an angle of 45°.*

Shift direction	Shift [mm]	Measured dose [cGy]	Passing rate [%]	CT Similarity	$\Delta_{passing\ rate}$ [%]	$\Delta_{dose,chamber}$ [%]
Reference	0	203.81	99.96	0.99	0.00	0.00
Transversal	20	195.42	90.08	0.92	9.88	4.12
	25	187.63	88.69	0.91	11.28	7.94
Longitudinal	20	203.81	99.92	0.99	0.04	0.00
	40	67.14	99.75	0.99	0.21	67.06
Vertical	20	196.62	90.29	0.93	9.68	3.53
	30	139.67	87.83	0.90	12.14	31.47
Rotation	15	201.42	99.88	0.99	0.08	1.18
	35	82.72	99.91	0.99	0.05	59.41

The greater shifts lead, as expected, to gamma failures in transversal and vertical direction. However, "TomoGamma" was not able to detect any change in longitudinal direction, whereas the ionization chamber detected the shift of 40mm. The smaller rotation remained undetected in all conducted measurements. Only the ionization chamber was able to detect the change of 35°. "TomoGamma" had a better sensitivity for all shifts, except for the rotations, the greater vertical, and the greater longitudinal shifts.
In general, the gamma analysis failed when the measured dose exceeded a difference of 2% as well, except the 40mm longitudinal shift.
The results of the fit can be found in table 5.15.

5.3.1.4 Cheese with a heterogeneous configuration

The next three tests were performed with the following density variations: air (0g/cm^3), adipose tissue (0.943g/cm^3), breast tissue (0.980g/cm^3), and inner bone (1.152g/cm^3). The configuration can be seen in figure 5.7.
These tests are closer to real scenarios, since the human body consists of a variety of different tissues and structures with varying electron densities. Due to the latter, the penetrating photons have more or less interactions with the matter and thus it is expected smaller variations of the test setup will be detectable.

Figure 5.7: *The configuration of the density plugs used in the tests of the heterogeneous setup of the cheese phantom.*

Off-centered PTV, three OARs

For the first test a cylindrical target with a diameter and length of 6cm each was created. It was positioned at (5.66cm, 5.66cm). Two plugs were contoured as OARs plus an additional cylindrical OAR at the center having a diameter and length of 6cm each. The PTV does not overlap with the heterogeneities.

Table 5.8: *Results of the test with an off-center positioned target and three cylindrical OARs. The OARs and the target are not overlapping.*

Shift direction	Shift [mm]	Passing Rate [%]	CT Similarity [%]
Reference	0	99.89	0.99
Transversal	10	98.59	0.96
	20	89.91	0.92
Longitudinal	10	99.45	0.99
	20	99.04	0.99
Vertical	10	93.29	0.96
	20	86.91	0.93
Rotation	10	99.34	0.99
	20	98.72	0.99

The larger shifts of 20mm in transversal and vertical direction could be detected by the gamma analysis and the CT comparison. Additionally, the 10mm displacement in vertical direction was flagged red. The CT similarity already created a warning signal for the minor shifts in both transversal and vertical direction.
Applying a curve fit, it was concluded that shifts larger than 15mm in transversal and 8mm in vertical direction can be detected by the gamma analysis. The sensitivity of the CT

comparison is 12mm in both directions. The values of the ionization chamber are missing, since it was broken at the time of the measurement.

Off-centered PTV, three OARs

The next test is almost identical to the previous one, but with the important change that the target is now at (-5.66cm, 5.66cm), thus overlapping with the inserted heterogeneities. This setup and configuration simulates the worst case scenario, since the unexpected change in anatomy is happening at the primary location of the dose distribution. Thus, minor changes should have greater influences on the planned data.
It was decided to decrease the step size in this test, since it is posing the biggest medical challenge. That is why it is important to know when which factor starts to signal an error.

Table 5.9: *Results of the test with an off-center positioned target and three cylindrical OARs. The heterogeneities and the target are now overlapping.*

Shift direction	Shift [mm]	Measured dose [cGy]	Passing rate [%]	CT Similarity	$\Delta_{passing\ rate}$ [%]	$\Delta_{dose,chamber}$ [%]
Reference	0	88.66	99.87	1.00	0.00	0.00
Transversal	5	93.23	95.81	0.98	4.06	5.15
	10	96.28	91.20	0.95	8.68	8.59
	15	99.32	88.19	0.92	11.70	12.03
	20	104.20	86.01	0.90	13.87	17.53
Longitudinal	5	75.56	99.88	1.00	0.01	14.78
	10	57.77	99.77	0.98	0.09	34.85
	15	41.56	94.18	0.95	5.69	53.13
	20	23.64	83.24	0.91	16.65	73.33
Vertical	5	93.23	98.51	0.98	1.36	5.15
	10	95.67	96.13	0.95	3.74	7.90
	15	98.10	93.87	0.93	6.01	10.65
	20	97.49	91.68	0.90	8.20	9.97
Rotation	10	72.51	93.28	0.98	6.60	18.21
	20	59.23	89.61	0.97	10.27	33.20
	30	50.94	88.66	0.96	11.22	42.54
	40	43.99	89.65	0.97	10.23	50.38

As expected, smaller errors in positioning can be detected with heterogeneities in the target volume. All changes in the rotation were detected. In transversal direction the 5mm shift was not red flagged but is already down to a passing rate of 95.8%. The ionization chamber was capable of detecting already the smallest applied variation and had a better

sensitivity throughout the whole test.
Once again doing a curve fit, the following detection thresholds could be determined:

Table 5.10: *Failure thresholds for the experiment where the target volume is overlapping the heterogeneities.*

	Transversal [mm]	Longitudinal [mm]	Vertical [mm]	Rotational [°]
Gamma analysis	6	15	13	7
CT similarity	10	15	11	40

Adding heterogeneities without displacements

The ROIs, their contours and the positions, remained unchanged in comparison to the previous setup. In order to test the detection efficiency with heterogeneities, density plugs of air and lung tissue, and a bolus of 2cm where added to the phantom. These tissues were selected since the observed anatomy changes are mainly respiration motion and changes in bowel gas.
These changes where measured individually and combined to see to which extend density changes have to be present for detection.

Table 5.11: *Results of the experiments where at first single heterogeneities were inserted and then in combination. No positional shifts were applied.*

Heterogeneity insert	Measured dose [cGy]	Passing rate [%]	CT Similarity	$\Delta_{passing\ rate}$ [%]	$\Delta_{dose,chamber}$ [%]
none	112.58	99.86	1.00	0.00	0.00
Air	116.84	98.57	0.99	1.29	3.78
Lung	111.97	99.06	0.99	0.80	0.54
Lung+Air	116.84	97.42	0.99	2.44	3.78
Bolus 2cm	102.24	81.50	0.98	18.38	9.19
Lung+Air+Bolus	106.50	89.25	0.98	10.63	5.41

One can see that neither air nor lung tissue create a failing gamma passing rate. Only when the bolus is added to the setup the gamma analysis is signaling a failing analysis. The ionization chamber was able to detect the air gap and its combination with the lung density plug. However, "TomoGamma" proofed to have a better sensitivity in all other cases, although the CT comparison could not signal one single density variation.

5.3.1.5 Test series adding a bolus

Observing that the bolus has the biggest influence in the previous gamma analysis, it was decided to do an extra test series investigating its impact in more detail on the homogeneous cheese phantom.

Centered PTV, 2 off-centered OAR

The centered PTV has a 3cm diameter and a length of 3cm as well. The two OARs are at the coordinates (5.66,5.66) and (-5.66,5.66) having both a diameter and length of 6cm each.

Table 5.12: *Results of the experiments using the homogeneous setup of the cheese phantom in combination with bolus reductions. The PTV is positioned at the center and there are two OARs at 8cm distance from the center at an angle of 45° and 135°.*

Bolus reduction [cm]	Measured dose [cGy]	Passing rate [%]	CT Similarity	$\Delta_{passing\ rate}$ [%]	$\Delta_{dose,chamber}$ [%]
0	201.51	99.83	0.98	0.00	0.00
1	202.76	99.38	0.98	0.46	0.62
2	205.25	97.13	0.97	2.70	1.86
3	208.37	93.36	0.97	6.47	3.41

In comparison to the heterogeneous CIRS phantom (ct. table 5.3), where bolus differences of 0.7cm could be detected, the flagging with the homogeneous cheese begins at 2.6cm, which again can be explained by the small dosimetric changes with a homogeneous setup. Even the ionization chamber only has a difference larger than 2% at the reduction of 3cm.
Speaking of general sensitivity, "TomoGamma" is better in detecting the changes already giving a warning at a reduction of 2cm.

Centered PTV, cortical bone heterogeneity

The test setup remained mainly unchanged. Only a density plug having the same electron density as a cortical bone was inserted as heterogeneity.

Table 5.13: *Results of bolus reduction on a homogeneous cheese phantom with a cortical bone heterogeneity.*

Bolus reduction [cm]	Measured dose [cGy]	Passing rate %]	CT Similarity	$\Delta_{passing\ rate}$ [%]	$\Delta_{dose,chamber}$ [%]
0.00	207.24	99.95	0.99	0.00	0.00
0.50	212.62	100.00	0.98	0.05	2.59
1.00	217.40	98.61	0.96	1.34	4.90
1.50	223.37	95.92	0.95	4.04	7.78
2.00	229.34	92.34	0.94	7.61	10.66
2.50	235.91	88.55	0.93	11.41	13.83
3.00	241.88	85.61	0.92	14.35	16.71

One can see that adding only one heterogeneity already increases the detection efficiency, since a bolus reduction of 1.6cm will fail the gamma analysis. The warning level of the similarity parameters is decreased to a bolus reduction of less than 1cm.
The ionization chamber had a better sensitivity to the changes in all applied reductions.

Centered PTV, cortical bone heterogeneity, displacement

As a final test it was investigated how "TomoGamma" would react to a bolus reduction with heterogeneities present and arbitrary displacements. This scenario reproduces the realistic conditions of daily treatments.

Table 5.14: *Realistic reproduction of treatment deliveries: The bolus is reducing, while the phantom is moving with heterogeneities in the radiation path.*

Bolus reduction [cm]	Shift (x,y,z) [cm]	Measured dose [cGy]	Passing rate [%]	CT Similarity	$\Delta_{passing\ rate}$ [%]	$\Delta_{dose,chamber}$ [%]
0.00	(0,0,0)	207.49	99.76	0.98	0.00	0.00
0.50	(4,0,3)	209.28	99.84	0.97	0.07	0.86
1.00	(2,0,7)	206.29	99.27	0.96	0.49	0.58
1.50	(5,0,3)	200.31	98.40	0.94	1.36	3.46
2.00	(4,0,4)	171.01	96.99	0.92	2.79	17.58

Although a gamma failure could not be provoked in this test, "TomoGamma" is still sufficient enough to detect changes as soon as the ionization chamber due to the CT comparison. Even the ionization chamber could not detect a smaller reduction either, whereas the similarity parameter at least signaled a warning.

5.4 Considerations of the sensibility of "TomoAdaptive"

During this work, we did not assess the influence of uncertainties on the sensitivity of "TomoAdaptive" due to time constraints, because we preferred to go on and test clinical cases.
Still, it is recommended in future work to conduct the following tests:

- A physician should approve the changes of the ROI geometry done by the deformable registration.
- Although 21st Century Oncology validated the dose calculation against the TPS of TomoTherapy, the information given in the DVHs should be verified by comparing the dose information to measurements of an ionization chamber for various setups.

5.5 Summary of the assessment

Table 5.15 summarizes the thresholds for failing gamma analyses derived from the curve fits based on the previously presented tests. Additionally, some warning thresholds creating a yellow flag are shown below in the table for the test cases closest to real treatment scenarios.
In homogeneous setups, the gamma analysis may not have enough sensitivity. It indicates a problem starting with shifts bigger than 1cm in the best case and theoretically 2m, based on the curve fit, in the worst case, which is larger than the treatment couch itself. Nevertheless, "TomoGamma" is performing well by using the similarity parameter, which creating a warning starting with shifts bigger than 5mm. In comparison to an ionization chamber, "TomoGamma" had a better sensitivity in the homogeneous test series.
Introducing heterogeneities, the gamma analysis is more reliable in detecting shifts. It creates a warning with shifts larger than 6mm, whereas the CT comparison is able to detect a difference starting with 10mm. Although, "TomoGamma" was not as sensitive as the ionization chamber in these tests, it is still sufficient by at least creating a warning signal, when the chamber measured a bigger difference than 2%.
In the last test measurements with a bolus "TomoGamma"'s sensitivity is comparable to the ionization chamber's detection efficiency.

As overall conclusion, it can be stated that "TomoGamma" is sensitive enough for ap-

plication on clinical cases as long as all provided parameters are considered. By doing so, one is able to detect treatment errors caused by heterogeneities, positional or anatomical changes as efficient as with an ionization chamber.
Furthermore, it is recommended to use a gamma criterion of 2%/2mm, since the acceptance of bigger differences will probably lower the sensitivity to the centimeter-range.

Table 5.15: *Overview of the obtained thresholds when the passing criterion will be smaller than 95%. The values are given in the directions: transversal, longitudinal, and vertical. At the bottom are the calculated thresholds when the yellow flags as a first warning a starting to occur for the gamma analysis.*

	RANDO	Cheese homogeneous			Cheese heterogeneous			Cheese Bolus			CIRS
		centered PTV, no OAR	centered PTV, OAR	off-center PTV, OAR centered	PTV off-centered, 3OARs	PTV off-centered overlapping heterogeneities, OAR in center	Different heterogeneities	OAR off centered, OAR ring	OAR vol interd.	displacement	
Gamma failure [mm]	19, 28.85, 19.19	88.96, 609.00, 51.06	219.40, 509.5, 191.9	10.50, 613.00, 9.24	14.97, 103.5, 7.59	5.71, 14.52, 12.49	only all-in detected	26	16	25,7	7.02
CT similarity failure [mm]	5.78, 8.11, 6.09	12.3, 70.67, 12.16	11.06, 27.30, 12.17	13.00, 83.58, 15.00	12.40, 401.4, 12.18	10.08, 14.90, 10.60	not detected	not detected	15	11.7	N/A
Rotation (γ, CT) [°]	19.87, 12.94	N/A	1966, 83.58	197.1/ 610.5, 775.3	78/380	7.10, 40.16		N/A	N/A	N/A	N/A
Yellow flag	7.97, 21.87, 9.62				11.7, 51.71, 3.75	2.99, 12.75, 6.60					5.40

5.6 Assessing uncertainties with the help of "TomoGamma"

Equipped with a good in-vivo dosimetry (IVD) system, one can now start further investigations on uncertainties present during TomoTherapy treatment deliveries to see how stable a treatment plan is over time and to see the influence of uncertainties.

5.6.1 Fraction by fraction development of the passing rate

It is too complicated to perform daily IVD with conventional linear accelerators. Setting up the measurement, even using the EPID, takes too much time and the following analysis occupies the physicist for a long time. That is why, at the Institute Curie, IVD on c-arm accelerators is only done the first three fractions and then once per week, although it is advised to do it more frequently (Celi (2016)).
The benefit of "TomoGamma" is that all these processes are automated and done in the background without additional workload during the treatment delivery. Therefore, daily delivery checks were implemented to answer the following questions concerning the general development of the delivery:

1. Are there substantial changes in the gamma passing rate, i.e. in the quality of the treatment delivery, both between consecutive fractions and between the first and last fraction?

2. Is it possible to determine a certain fraction number when a general revision of the delivery plan should be done?

The gamma passing rates of all investigated fractions were extracted using an in-house developed extraction program written in Matlab. The study comprised both matched TomoTherapy units and all tumor localizations. Thus, 359 RT plans of Tomo1 and 227 plans of Tomo2 were included. Two tests were done:

- All fraction numbers were averaged to create one average "plan". From this plan the gradient of a trend line was calculated.

- A trend line of each single plan was calculated and their gradients were then averaged.

5.6.1.1 Results

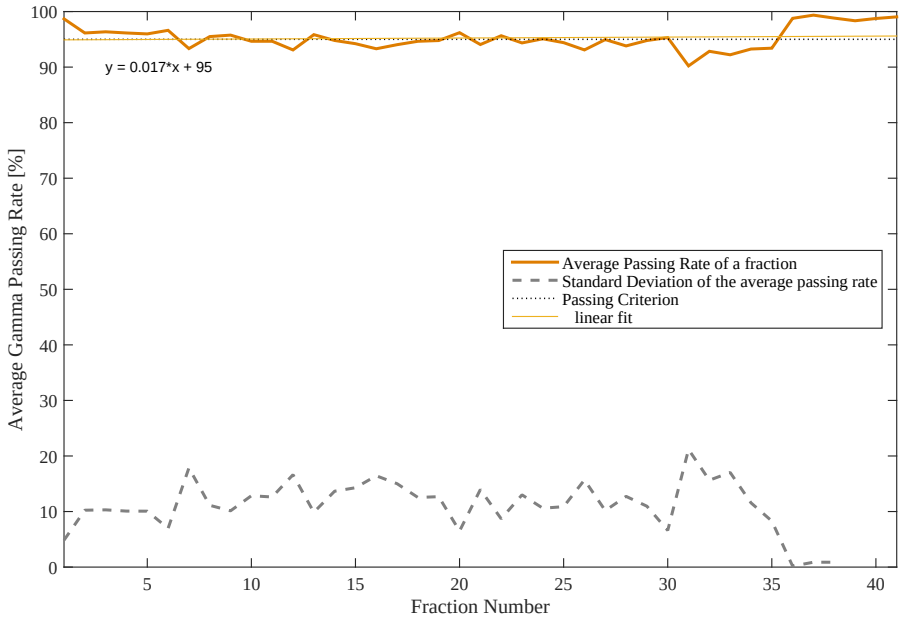

(a) Tomo1

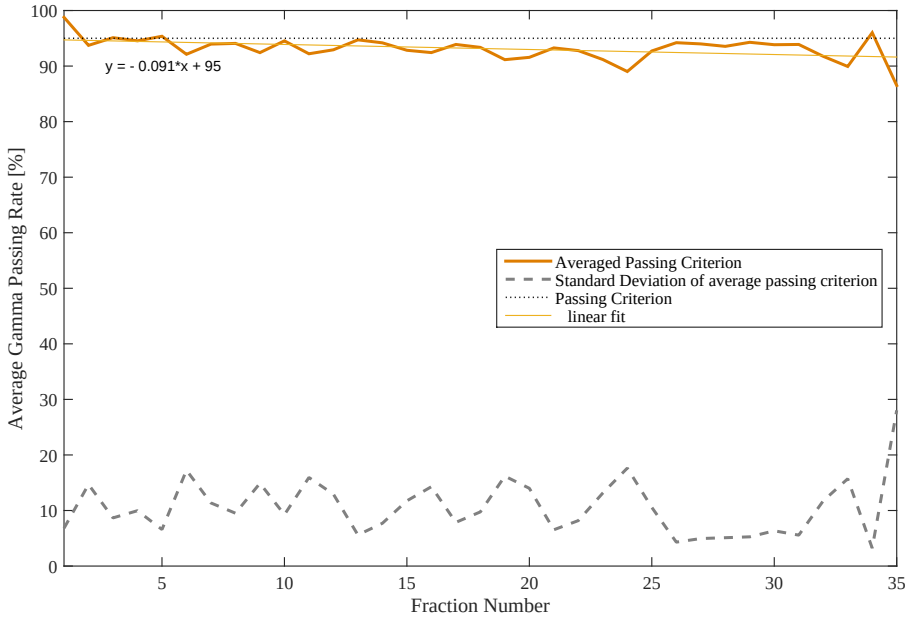

(b) Tomo2

Figure 5.8: *Results of the averaged gamma results of Tomo1 (a) and Tomo2 (b).*

Table 5.16: *Results of the different obtained gradients evaluating the development over time of the gamma analysis.* $m_{averaged\ fractions}$ *is giving the gradients obtained by applying a linear fit to the averaged gamma passing rates of each fraction.* $\bar{m}$ *is the average of all gradients calculated for each plan.*

	$m_{averaged\ fractions}$	$\bar{m}$	m<0	-0.5<m<0.5
Tomo1	0.02	-0.28	72.42%	76.32%
Tomo2	-0.09	-0.4	79.74%	72.25%

The linear fits of the averaged fractions show a low gradient. The one of Tomo1 is even positive due to the low sample size of plans having more than 35 fractions and the ones existing have a high passing rate.
Calculating the gradient of the plans individually and taking their average leads to different results: Both are negative and multiple times steeper. Tomo2 has more plans that have a negative gradient than Tomo1 and the averaged passing rates are lower in general. This might be caused by two factors. Although both units are matched in their output, they are used to treat different tumor localizations. Tomo2 delivers radiation to more complex cases like head and neck or pelvic tumors, whereas Tomo1 primarily treats prostate cases. The other reason might be that Tomo2 was more unstable than Tomo1. Reasons for the instability will be discussed in the next chapter.
In order to answer the questions mentioned above, it can be stated that there are no substantial differences in the passing rates and no fraction for general revision were found; although, it might be worth to check the behavior of the Tomo2 plans starting with fraction 17, i.e. after the delivery of around 50% of the planned fractions.

5.6.2 Machine Output

The reliable production of x-rays is a critical part of radiotherapy. Its procedure is strongly dependent on the digital and mechanical parts within the accelerator. It is thusly essential to test the machine output on a daily basis to verify whether the output is within the tolerance limits of the reference data. Additionally, other checks have to be done on a regular basis, called machine quality assurance (machine QA), ensuring that there are no major issues when starting a treatment.
However these measurements give a general overview and cannot assure that any error will occur at another point in time. After observing several failing DQAs, one can say that these failures seemed to occur sporadically, i.e. measuring the same plan a second time lead to passing DQAs. It was assumed that there is a problem with the output, but it was neither possible to reproduce the failing situation nor to verify the assumption.

Upon introducing "TomoGamma", it was noted that the first investigated cases had several failing fractions, with a passing rate lower than 95%. As mentioned above, "TomoGamma" is capable of extracting the machine output of each dose projection and calculating the dose rate. A further investigation showed that the majority of the failing plans did not pass the outputMean and sometimes the outputVar criteria (ct. table 5.2). Furthermore, it was observed that the dose rate drops considerably below the planned value probably causing the low passing rate, since the output and as such the applied dose was too low (ct. figure 5.9(a)).
Installing "TomoGamma" made it possible to find the root-cause of the existing problem of the QA at Institut Curie. In parallel, the vendor developed a system to control the machine output: The Dose Control System (DCS).
The DCS is a servo based closed loop control (Staton et al. (2012)) on the machine output. It employs the two built-in head ionization chambers as feedback sensors. Then, the output and as such the dose rate is stabilized by adapting the LINAC's accelerating current, so that the dose rate drift should not occur anymore (ct. figure 5.9(b)). An analysis was conducted comparing gamma passing rates before and after the installation of the DCS to verify the feature and as well to estimate how big the influence of the drop in the output was.

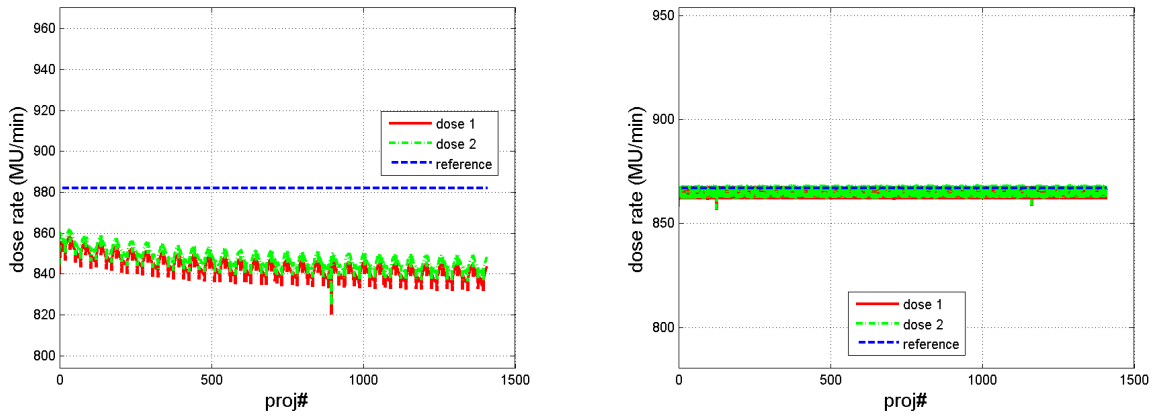

(a) (b)

Figure 5.9: *Results of the dose rate analysis of the same patient and same plan prior the DCS installation (a) and after it (b). dose 1 (red, solid line) and dose 2 (green, dashed line) are the data of the overhead ionization chambers and reference (blue, dashed line) is the planned value.*

5.6.2.1 Application on clinical cases

A total of 161 patients with different treatment sites were included in the study, therefrom 43 prior and 118 posterior to the installation of the DCS, leading to a total of 4253 analyzed fractions (1144 prior and 3109 posterior to the DCS installation).
The planned and delivered dose rate, and gamma passing rates were extracted from "TomoGamma" using an in-house written software created in Matlab®, which as well calculated the analyses.
Based on the previous assessment, it was decided to set the gamma criterion to 2%/2mm. The passing rate remains unchanged at 95%.

5.6.2.2 Results

When comparing the results of the two patient groups, the average gamma passing rate moved from 90.90% prior to the installation up to 94.79% after the upgrade of the Dose Control System. The average deviation of the measured dose rate compared to the planned value was 2.44% prior to DCS vs. 0.17% post DCS installation. This difference is smaller than expected and may be due to the fact that - in the absence of the DCS - the dose rate could shift. Depending on the magnitude of this shift, it may lead to a failure of the plan in IVD. Nevertheless, there is an obvious correlation between the deviation of the dose rate and the gamma passing rate: 60.18% of the plans have a passing rate superior to 95% with a variance of 10.69 after the DCS upgrade in contrast to 27.91% passing plans and a variance of the gamma analysis of 56.33 before the DCS. This is well reflected in our exemplary case from figure 5.9. Even with a routine gamma analysis of 3%/ 3mm the fractions prior the DCS upgrade have an average gamma passing rate of 59.85% and an average intra-fraction variance of the dose rate of 4.76 $[MU/min]^2$. After the installation, the average passing rate increases to 97.43% with an intra-fraction variance of 2.13 $[MU/min]^2$. In terms of differences to the planned dose rate, the value decreases from 4.25% to 0.08%.

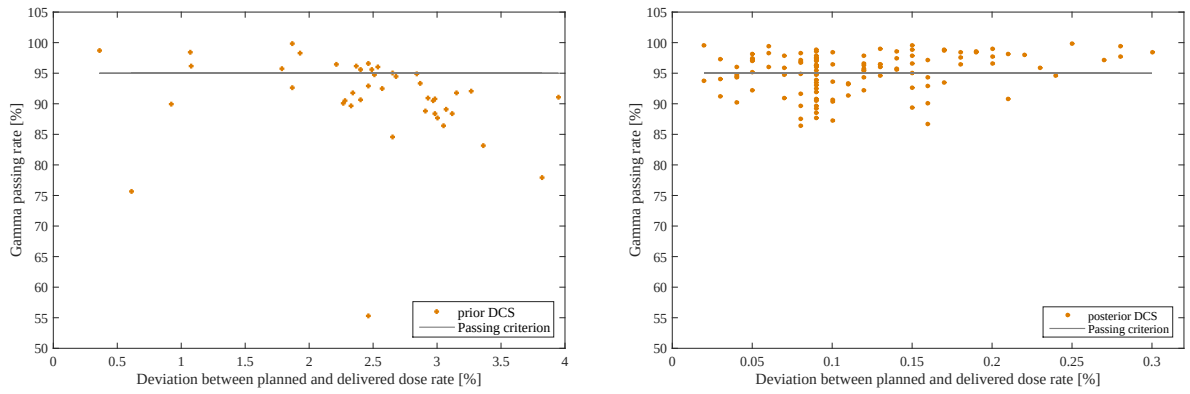

(a) (b)

Figure 5.10: *Results of the study investigating the influence of the dose rate drift on the gamma passing rate. Shown are the averaged passing rates prior (a) and posterior (b) the DCS installation of the analyzed plans.* ***Please note the different scale on the x-axis****. For the results after the upgrade the highest data point's value is even smaller than the smallest value for the cases prior the installation.*

As can be seen in figure 5.10, the gamma passing rate clearly decreases as soon as the deviation of the dose rate exceeds 2%. The newly installed DCS prevents this by keeping the deviation below 0.5%. The upgrade is thus doubling the passing rates and decreasing the variance of the dose rate to a fifth.
When focusing on a single patient affected by the dose drift, one can see that a possible underdosage could be prevented and gamma passing rates decreased above the passing criterion by using the DCS system.
Analyzing the causes of all failing gamma analyses, the dose drift is throughout the leading error source causing gamma passing rates below 95% for 25-83% of the analyzed fractions. In figure 5.11 one can see the influence in a direct comparison of failing fractions including and excluding cases where the drift was the primary error source.

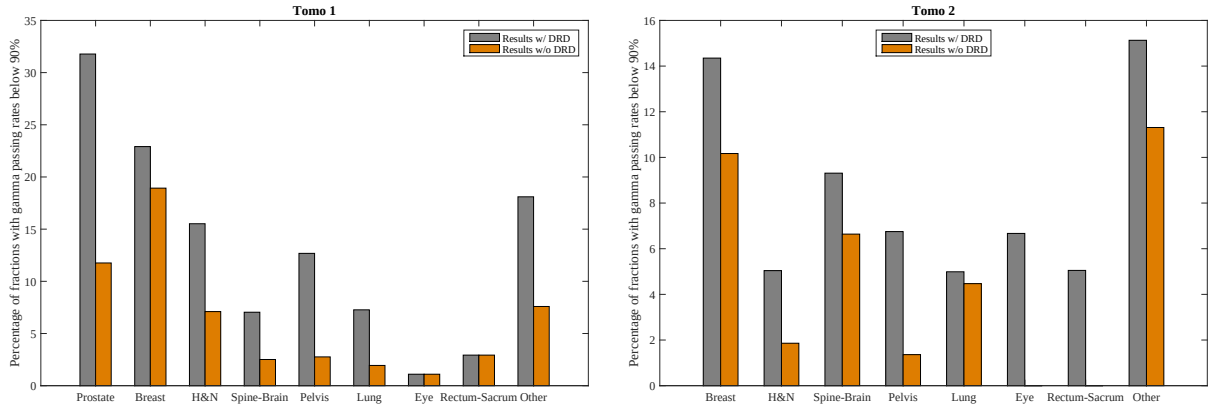

(a) (b)

Figure 5.11: *Shown is the influence of the dose rate drift (DRD) on the uncertainties for different tumor localizations. The uncertainty introduced by the drift is reduced to 50% using the DCS. For eye and rectal treatments at Tomo 2 it even drops to 0. Please remember that the units treat different locations, thus the x-axis in 8a9 and (b) is different.*

5.6.2.3 Discussion

With the help of "TomoGamma", it was shown that the Dose Control System is an important tool ensuring the quality of a treatment by stabilizing the machine output avoiding a potential underdosage of the target volume. The uncertainty based on the machine output could be reduced to 50%.

5.6.3 Additional uncertainties in TomoTherapy

Once we managed to remove the leading source of uncertainties of our TomoTherapy units, namely the machine output, a further analysis could focus on additional sources affecting the gamma analysis.
In order to do so, "TomoGamma" was applied on both TomoTherapy units leading to a total number of 577 RT plans (363 of Tomo 1 and 208 of Tomo 2) with various treatment sites. Each treatment site has its own set of error sources due to different heterogeneities or irregularities of the body.
The root-causes were assessed for each failing fraction; the conclusion was noted down in a summary table for all treatment sites, resulting in an overview of how often which uncertainty caused a gamma failure. Table 5.17 shows the results of the leading uncertainties sorted by main clinical localization assessed with "TomoGamma".

Table 5.17: *Final overview of the leading sources causing gamma passing rates below 95%. Combination expresses that at least two possible causes could be found. The dose rate drift (DRD) is in an extra column, since it is not occurring anymore, but was the leading cause before the DCS upgrade. The other columns show the results, when the DRD could be excluded as leading error source. The percentage value gives the proportion of red flagged plans caused by the corresponding source after the DCS installation.*

	Tomo 1			Tomo 2		
	Primary error source	Secondary error source	DRD	Primary error source	Secondary error source	DRD
Breast	Respiration (19.44%)	Combination (13.89%)	47.00%	Breast too big to be reliable reposi-tioned/ anatomy change (9.09% + 9.09%)	Combination (9.09%)	72.73%
H&N	Combination (45.83%)	Dental Implants (25.00%)	29.17%	Anatomy change (50%)	N/A	50.00%
Spine/ Brain	Anatomy change incl. Bowel gas (50.00%)	Combination (25.00%)	25.00%	Combination (50%)	N/A	50.00%
Pelvis	Combination (25.00%)	Anatomy change incl. Bowel gas (14.28%)	57.14%	Anatomy change (16.67%)	Combination (8.33%)	75.00%
Lung	Combination (25.00%)	N/A	7.00%	Anatomy change (75%)	N/A	25.00%
Eye	Anatomy change (50.00%)	N/A	50.00%	N/A	N/A	100.00%
Rectum	Anatomy change incl. Bowel gas (100.00%)	N/A	N/A	N/A	N/A	100.00%
Other	Combination (8.33%)	Error in position (8.33%)	83.33%	Hip implants (25%)	Combination (25.00%)	50.00%
Prostate	Hip implants (25.00%)	N/A	75.00%	N/A	N/A	N/A

In most of the cases, not a single uncertainty lead to the failure of the gamma analysis but rather a combination of at least two factors, e.g. weight loss of the patient combined with respiratory motion.

Metallic implants lead to artifacts in the radiologic images, thus disturbing the gamma analysis, so the information given by "TomoGamma" is not reliable.
Considering the respiratory motion it was observed that the gamma failure is often in the low dose region at the border of the body, e.g. the upper shoulder, but the gamma analysis in the region of the treatment volume was passing.

Knowing the leading error sources, it is possible to develop and introduce new localization-specific measures to reduce their influences on the quality of the treatment delivery. "TomoGamma" can help to assess their efficiency by continuously checking comparing the gamma analyses.

5.7 Offline Adaptive Radiation Therapy: Considerations of the use of Tomoadaptive and "TomoGamma" in clinical routine

Adaptive radiotherapy (ART) has been a difficult task, because many factors needed to develop to a certain point, e.g. computational power including parallel computing on GPUs for fast calculations for an affordable price or communication interfaces between treatment machine and analyzing software/ stations.
In order to fully implement ART in clinical routine, following criteria have to be fulfilled:

- Daily 3D-CT being registered to the planning kVCT allowing deformable registration to detect anatomy changes.
- Organ segmentation on the daily MVCT for updated DVHs.
- Dose calculation on daily MVCT to estimate what actually happened during the fraction (hotspots/ coldspots)
- Automatic workflow to minimize occupation of staff and allowing for time consuming calculations being performed in the background 24/7.

It is clear that "TomoGamma" and "TomoAdaptive" have the potential to offer the opportunity to start trials to do ART. For a practical protocol all patients being treated should be archived at least once every day. It is advised to archive treated patients twice per day, e.g. just before lunch break and after the last treatment, to ensure that results are ready the next day.

Alternatively, a recommended use case could be: The first "TomoGamma" results should be present within a few minutes after archiving the files. Then, one can check if there is an error leading to failing gamma passing rates and if these are being caused by technical sources, e.g. machine output or error in patient set-up.
One can review the DVHs in "TomoAdaptive" for the same fraction if no explanation could be found and then assess whether the dosimetric difference might be critical. Possible explanations might be found in changed patient anatomy, which can be checked in "TomoAdaptive" as well. Additionally, it allows seeing if the anatomical changes lead to critical hotspots in organs at risk or cold spots within the target volume.
Finally, with all these information one can decide whether replanning is necessary or not. The overall workflow is shown in figure 5.12.

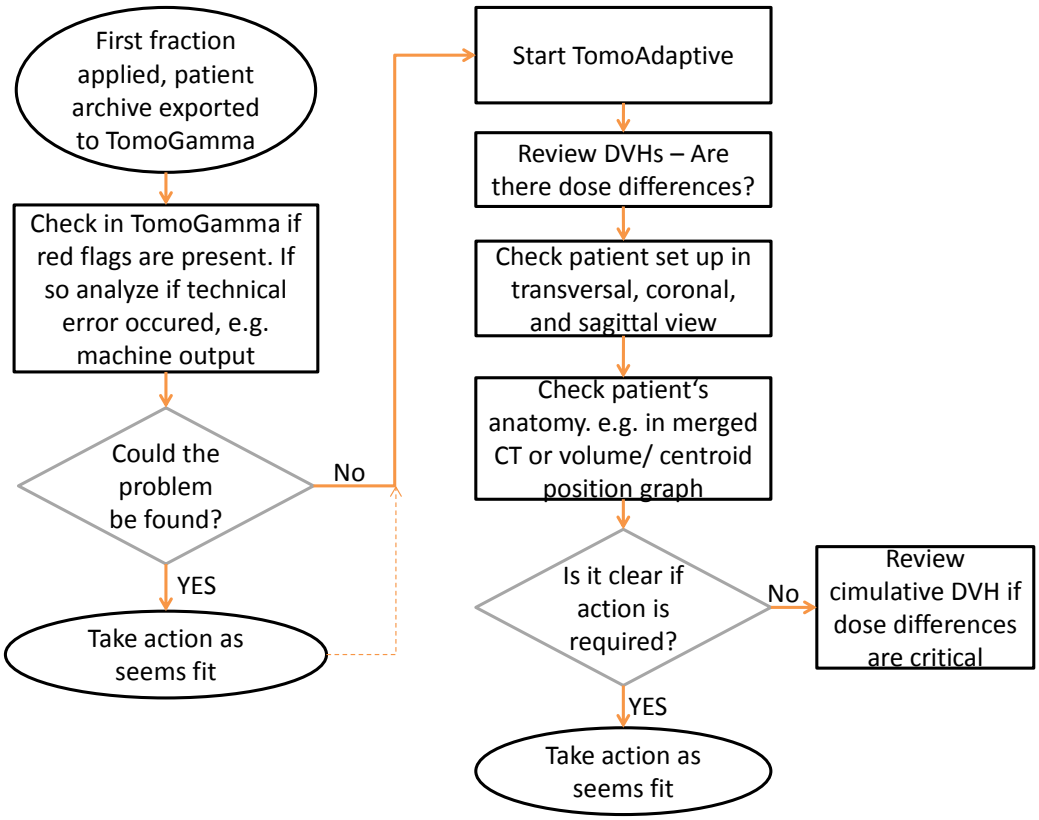

Figure 5.12: *Possible workflow of adaptive radiotherapy using "TomoGamma" and "TomoAdaptive".*

Up to this point, the additional workload is within an acceptable limit. The export process can be a batch process. The calculations are then started automatically and it is only necessary to take some time to review the results.
However, should replanning be necessary, the workload increases exponentially due to

safety protocols leading the treatment chain to start from scratch: A new planning CT has to be done, new contouring, a new plan, all signatures by physicians and physicists, and finally another DQA before the new plan can be applied.
The question to be answered in the future is: How big must the difference be to justify replanning?

It is clear that the implementation of Adaptive Radiotherapy in routine requires speed and automatization. First developments already go into this direction, e.g. automated contouring or automatically setting the treatment plan objectives in the TPS. Another good approach to speed up the DQA measurement is the proposed approach of phantom-less DQA (Pisaturo et al. (2015)). The procedure works without setting up, and positioning a phantom and dosimetric utilities leaving out the warmup phase and measuring the background noise. Thus, only the actual radiation time is remaining.

5.8 Summary and Conclusions

The aim of this chapter was to assess globally the uncertainties present in TomoTherapy. After successfully benchmarking the important tool, it was possible to get an idea what is actually happening during a treatment delivery. It was found that, based on all analyzed characteristics, one is capable of detecting changes in the position of 5mm when the first warning in form of a yellow flag is created. Position shifts of larger than 10mm will create a critical alert using a gamma criterion of 2%/ 2mm.
Verifying the treatments on a daily basis, it can be seen that the dosimetric output of the machine was not sufficiently stable. The dose rate drift was not big enough to provoke an emergency stop by the interlocks regulated by the head chambers. Nevertheless, it was big enough to lead to multiple failures in the gamma analysis, and therefore indicating a potential underdosage. Seeing these effects, it seems vital to upgrade a TomoTherapy unit with the Dose Control System to avoid single cases affected negatively by the DRD. Using "TomoGamma", it was proven that the DCS is working well and reduces the variation of the output to a minimum.
With the biggest uncertainty eliminated, a broad study of uncertainties with reference to specific tumor localizations could be done. Two major sources leading to low passing rates are anatomical changes of the patient, e.g. different amount of bowel gas or size of the bladder between single fractions, and combination of two or more uncertainties, e.g. a big breast which is difficult to reposition and respiratory motion.
Being aware of the leading causes of gamma failure, one is now able to go further and to

adapt the existing safety protocols, e.g. gas releasing rectal balloons for prostate cases. Finally, it was shown how tools like "TomoGamma" and "TomoAdaptive" can be developed further to implement adaptive radiotherapy in clinical routine. The checks of the treatment delivery can be done fast and easily due to the automated flagging system. The next step will be to create new protocols and infrastructures to speed up the process of replanning.

Chapter 6

General Conclusions and Outlook

As mentioned in the introduction, uncertainties occur along the complete workflow a patient undergoes when treated in external beam radiotherapy. This work approached some of them in the three main sections: pre-treatment QA, assessing overmodulation during the delivery, and IVD in TomoTherapy as a follow-up of a treatment delivery.
Initially, we demonstrated that assessing the quality and accuracy of the QA measurement chain plays a major role in further understanding other sources of uncertainties in radiotherapy. It was shown that the angular dependency of 2D chamber arrays is a non-negligible effect affecting the measurement equipment. The presented approach for TomoTherapy units is performing a theoretical synchronization of the measured snaps with the gantry angle by introducing a virtual gyroscope. Despite the positive results, one might argue if the synchronization is good enough. A bigger sample size of patients will verify the fail-safety of the algorithm. Though, it might be beneficial to use the proposition of phantomless DQA directly using the built-in detectors as proposed by Pisaturo et al. (2015) and lately developed by 21st Century Oncology. Such a solution is improving the position uncertainty of the detector and the angular dependency. It would be mandatory though to periodically verify the detector signal quality.
The assumption that the modulation of dual arc VMAT prostate cases causes DQA failures was not be completely confirmed. The results showed that the investigated cases have a rather low modulation, hence other tumor localizations should be included in future studies. Publications studying a variety of tumor sites came to the conclusions that there is also no clear threshold marking an overmodulation (Masi (2013), Celi et al. (2015)). However, they found a tendency between the modulation and the DQA/ IVD results. Due to the large interest in investigating the complexity of treatment plans, it might be only a matter of time when a suitable factor can be confirmed. The publication of Valdes et al. (2016)

shows that the tested parameters are playing a role but need to be assessed and combined in a different way.
The last chapter introduced a new framework for IVD in TomoTherapy. It is based on the information collected by the on-board detectors and protocols and calculates amongst others a local gamma analysis. This application, "TomoGamma", provides useful information to assess if an error occurred during a treatment delivery. The sensitivity of "TomoGamma" is good enough to detect 0.5cm positional shifts if a gamma criterion of 2%/2mm is used. Applying the program in clinical routine it was possible to detect the root-cause of failing DQAs, namely the dose rate drift. After the installation of the Dose Control System, "TomoGamma" could confirm the improvement on the machine output, practically eliminating it as one of the leading error sources.
Furthermore, "TomoGamma" was used to create a first comprehensive summary of root-causes of delivery failures and to derive their influence on the treatment quality for a group of representative clinical localizations. Additionally, a second application was introduced in clinical routine: "TomoAdaptive". Both work complementary: "TomoGamma" is detecting a problem with a treatment delivery and "TomoAdaptive" is utilized to assess the clinical impact and if a replanning is necessary. This combination is laying the foundation of the introduction of adaptive radiotherapy in TomoTherapy, since it is assessing each treatment fraction automatically day-by-day.
As soon as the validation in clinical conditions of the deformation algorithm of "TomoAdaptive" is done, further investigations will be completed. One example might be a study of the volume change of, e.g. the breast, during radiotherapy application. Interfraction uncertainties, like the organ motion, can be assessed easily by extracting the information of the output file provided by "TomoGamma".

The presented work showed multiple uncertainties and how they can be assessed, resolved, or at least mitigated. As such, it aligns with the works ongoing in parallel in multiple institutions and publications on the subject. New technologies and techniques will come with new uncertainties or they will make it possible to be more accurate and reducing uncertainties. "TomoGamma" and "TomoAdaptive" are a good example of how new solutions can identify treatment problems to improve them increasing the treatment quality.

Bibliography

Agency I.A.E. 2000 Lessons learned from accidental exposures in radiotherapy. *Safety Report Series No.17* .

Ahnesjö A. 1989 Collapsed cone convolution of radiant energy for photon dose calculation in heterogeneous media. *Med. Phys.* **16** 577.

Arno J., Mundt J. and Roeske C. 2005 *Intensity Modulated Radiation Therapy*. Hamilto, London: BC Decker Inc.

Autorite de surete nucleaire 2014 *Patient safety paving the way for progress*.

Celi S. 2016 *Development and application of a multi-modality inverse planning system*. Ph.D. thesis, Universite Paul Sabatier.

Celi S., Wessels C. and Francois P. 2015 SU-E-T-685: Root Cause Analysis of in Vivo Dosimetry Controls for Dynamic Arc Treatments. *Med. Phys.* **42**(3) 3494.

Chofor N., Looe H., Kapsch R., Harder D., Willborn K., Rühmann A. and Poppe B. 2007 Characterization of the radiation quality of 60 Co therapy units by the fraction of air kerma attributable to scattered photons. *Phys. Med. Biol.* **52**(7) N137.

Dokic I., Mairani A., Niklas M., Zimmermann F., Chaudhri N., Krunic D., Tessonnier T., Ferrari A., Parodi K., Jäkel O., Debus J., Haberer T. and Abdollahi A. 2016 Next generation multi-scale biophysical characterization of high precision cancer particle radiotherapy using clinical proton, helium-, carbon- and oxygen ion beams. *Oncotarget* **7**(35) 56676.

Dong P., Lee P., Ruan D., Long T., Romeijn E., Yang Y., Low D., Kupelian P. and Sheng K. 2013 4Pi Non-Coplanar Liver SBRT: A Novel Delivery Technique. *Int. J. Radiat. Oncol. Biol. Phys.* **85**(5) 1360–1366.

Ezzell G., Burmeister J., Dogan N., LoSasso T., Mechalakos J., Mihailidis D., Molineau A., Palta J., Ramsey S.B. C.R., Shi J., Xia P., Yue N. and Xiao Y. 2009 IMRT commissioning: Multiple institution planning and dosimetry comparisons, a report from AAPM Task Group 119. *Med. Phys.* **36** 5359.

Forsberg D., Eklund A., Andersson M. and Knutsson H. 2007 Phase-Based Non-Rigid 3D Image Registration: From Minutes to Seconds Using CUDA. *Linköping University* URL `http://liu.diva-portal.org/smash/get/diva2:506435/FULLTEXT01.pdf`.

Freund L. 1897 Ein mit Röntgen-Strahlen behandelter Fall von Naevus pigmentosus piliferus. *Wiener Medizinische Wochenschrift* .

Hall E. and Giaccia A. 2011 *Radiobiology for the Radiologist*. Baltimore, Philadelphia: Lippincott Williams & Wilkins.

Hanusova T., Vondracek V., Badraoui-Cuprova K., Horakova I. and Koniarova I. 2015 New method for estimation of fluence complexity in IMRT fields and correlation with gamma analysis. *Journal of Physics: Conference Series* **573**(1) 012056.

Hofmann K. 2011 Implementation of a dose delivery modality using dynamic multileaf collimation and its application for real–time tumor tracking. *University of Heidelberg* .

IBA Dosimetry GmbH 2009 URL `http://test.scanditronix-wellhoefer.com/MULTICube.1362.0.html`.

Institut de Radioprotection et de Surete Nucleaire 2015 *Les accidents de radiotherapie*. URL `http://www.irsn.fr/FR/connaiscances/Sante/applications-medicales/accidents-sanitaires/accidents-radiotherapie/Pages/1-Qu_est-ce_qu_un_accident_de_radiotherapie.aspx?dId=2ecb1c79-375d-4849-9640-cd366950b6a5&dwId=22eb68db-0e12-49ba-a586-87439fbbb552#.Vb-xfZed5ng`.

Institut National Du Cancer, 2008 *Guide pour la pratique quotidienne de la Dosimetrie in Vivo en radiotherapie externe*.

Khan F. 2009 *The Physics of Radiation Therapy*. Baltimore, Philadelphia: Lippincott Williams & Wilkins.

Klein E.E., Hanley J., Bayouth J., Yin F.F., Simon W., Dresser S., Serago C., Aguirre F., Ma L., Arjomandy B., Liu C., Sandin C. and Holmes T. 2009 Task Group 142 report: quality assurance of medical accelerators. *Med. Phys.* **36** 4197–4212.

Kruse J.J. 2010 On the insensitivity of single field planar dosimetry to IMRT inaccuracies. *Med. Phys.* **37**(6) 2516–2524.

Latifi K., Zhang G., Stawicki M., van Elmpt W., Dekker A. and Forster K. 2013 Validation of three deformable image registration algorithms for the thorax. *J. Appl. Clin. Med. Phys.* **14**(1).

Low D., Harms W., Mutic S. and Purdy J. 1998 A technique for the quantitative evaluation of dose distributions. *Med. Phys.* **25**(5) 656–661.

Masi L. 2013 Impact of plan parameters on the dosimetric accuracy of volumetric modulated arc therapy. *Med. Phys.* **40**(7).

McNiven A., Sharpe M. and Purdie T. 2010 A new metric for assessing IMRT modulation complexity and plan deliverability. *Med. Phys.* **37** 505–515.

Oyewale S. 2013 Dose prediction accuracy of collapsed cone convolution superposition algorithm in a multi-layer inhomogenous phantom. *International Journal of Cancer Therapy and Oncology* **1**(1).

Pisaturo O., Mieville F., Tercier P.A. and Alla A.S. 2015 An efficient procedure for tomotherapy treatment plan verification using the on-board detector. *Phys. Med. Biol.* **60**(4) 1625–1639.

Plumat J., Andersson M., Janssens G., de Xivry J.O., Knutsson H. and Macq B. 2009 Image registration using the Morphon algorithm: an ITK implementation. *Université Catholique de Louvain* URL `http://liu.diva-portal.org/smash/get/diva2:343980/FULLTEXT01.pdf`.

Podgorsak E. 2005 *Radiation Oncology Physics: A Handbook for Teachers and Students*. Vienna: International Atom Energy Association.

Sekar Y., Thoelking J., Kuncoro Sihono D., Lohr F., Wenz F. and Wertz H. 2016 Characterization and clinical evaluation of a novel 2D detector array for conventional and flattening filter free (FFF) IMRT pre-treatment verification. *Unpublished* .

Shimohigashi Y., Araki F., Tominaga H., Sakata J., Kawasaki K., Kanetake N., Iwashita Y., Yoshimura S., Kawakami T. and Ishihara T. 2012 Angular dependence correction of MatriXX and its application to composite dose verification. *J. Appl. Clin. Med. Phys.* **13**(5).

Staton R., Biddle J., Langen K. and Meeks S. 2012 Evaluation of Dose Control System Performance on a TomoTherapy Hi-Art System. *Med. Phys.* **39** 3789.

System T.T. 2011 *Product Specifications*. Accuray Incorporated.

Valdes G., Scheuermann R., Hung C., Olszanski A., Bellerive M. and Solberg T. 2016 A mathematical framework for virtual IMRT QA using machine learning. *Med. Phys.* **43** 4323.

van Herk M. 2004 Errors and margins in radiotherapy. *Seminars in radiation oncology* **14** 52–64.

— 2011 *Margins and margin recipes*. URL `https://www.aapm.org/meetings/2011SS/documents/vanherk_aapmsummerschool2011.pdf`.

Webb S. 2003 Use of a quantitative index of beam modulation to characterize dose conformality: illustration by a comparison of full beamlet IMRT, few-segment IMRT (fsIMRT) and conformal unmodulated radiotherapy. *Phys. Med. Biol.* **40**(14) 2051–2062.

Wolfsberger L.D., Wagar M., Nitsch P., Bhagwat M.S. and Zygmanski P. 2010 Angular dose dependence of Matrixx TM and its calibration. *Med. Phys.* **11** 3057.

World Health Organization 2008 *Fact sheet No.297*. URL `http://www.who.int/mediacentre/factsheets/fs297/en`.

Wrangsjö A., Pettersson J. and Knutsson H. 2009 Non-Rigid Registration Using Morphons. *Linköping University* URL `http://citeseerx.ist.psu.edu/viewdoc/download?doi=10.1.1.95.4606&rep=rep1&type=pdf`.

Xu S., Xie C., Ju Z., Dai X., Gong H., Wang L. and Yang J. 2010 Dose verification of helical tomotherapy intensity modulated radiation therapy planning using 2D-array ion chambers. *Biomed Imaging Interv Journal* **6**.

Yang Y., Li T., Yuan L., Ge Y., Yin F.F., Lee W.R. and Wu Q.J. 2015 Quantitative comparison of automatic and manual IMRT optimization for prostate cancer: the benefits of DVH prediction. *J. Appl. Clin. Med. Phys.* **16**(2).

List of Figures

List of Tables

Flowcharts of created algorithms

Figure 6.1: *Workflow of a standard DQA measurement (black) and the additional portion doing the angular correction (grey).*

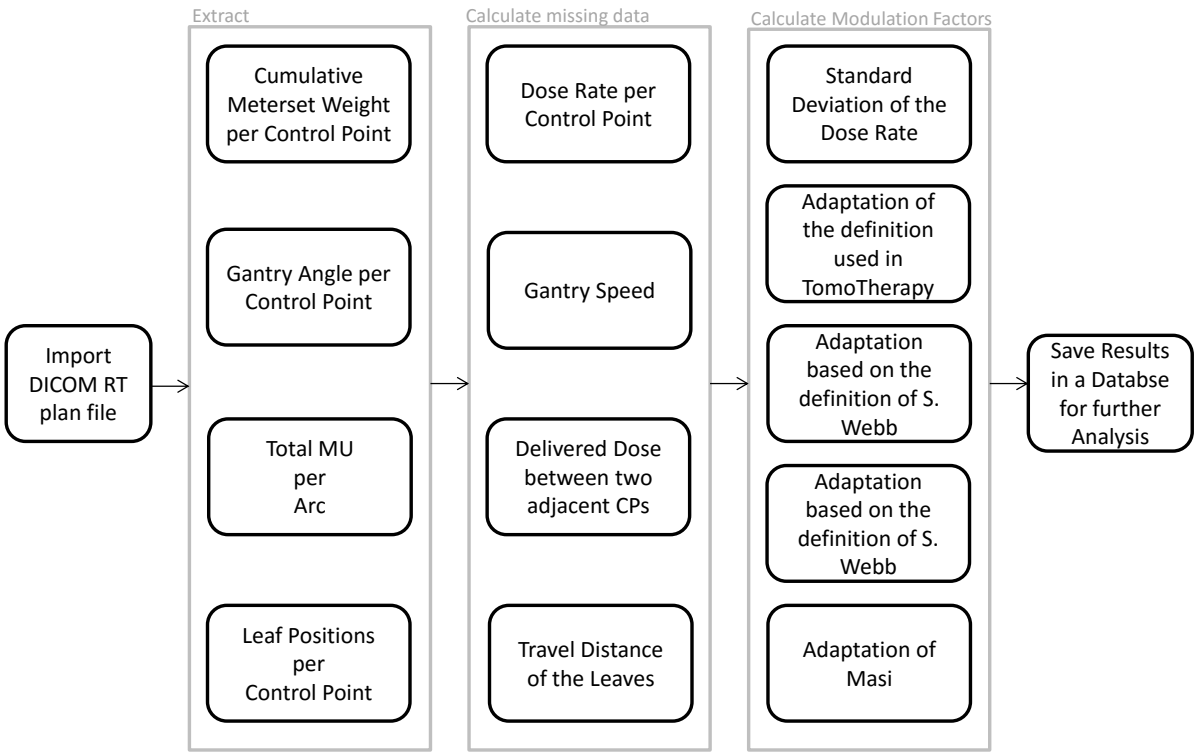

Figure 6.2: *Flowchart of the algorithm, which calculates the different modulation factors based on the data extracted from the DICOM plan file.*

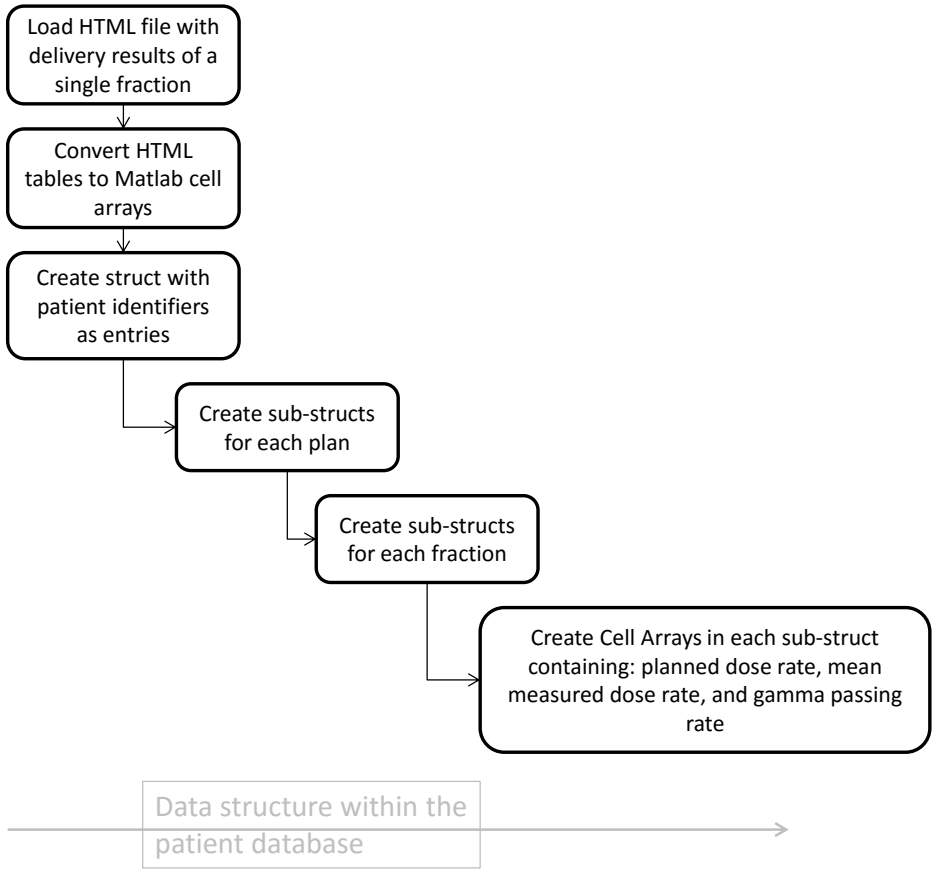

Figure 6.3: *Flowchart showing how the data of TomoGamma is extracted and transformed in a patient database containing the necessary information to conduct the work shown in chapter 5.*

Acknowledgements

I would like to thank Prof. Dr. Uwe Oelfke for accepting me as his PhD student, although the circumstances where not the easiest ones.

I would like to thank as well Prof. Dr. Joao Seco for his valuable time when assessing my thesis.

Furthermore, I would like to thank Prof. Dr. Hans-Christian Schultz-Coulon and Prof. Dr. Tilman Plehn for accepting to participate at my PhD defense.

One important role of this work was the one of Dr. Alejandro Mazal, whose relentless effort made this project possible. His caring attitude towards the students working in his department really surpasses the definition of a supervisor! Thank you very much Alejandro.

I want to express my gratitude to Dr. Sandra Losa and Dr. Jean-Luc Dumas. Thank you Sandra for being ready to help with everything at any time no matter the inconveniences for yourself.
Thank you Jean-Luc for your inspiration and input to this work, which strengthened the foundation of this thesis.

Another important character I want to thank is Sylvie Martin. One says that the real power of a department lies in the hands of the secretary, which is clearly your case. Thank you for helping with overcoming all the administrative obstacles, and for finding Alejandro wherever he was on this planet ;)

Thank you as well to Pascal Debruyne, who fought together with Alejandro, so I could survive living in Paris.

Of course I want to thank as well the team of the service of medical physics for the nice and welcoming atmosphere, especially thank you to Florence Wetta, Sabah Krim, Daniel Monteiro, Ahmed Hadji Henni, Julien Demoucron, and Noelle Pierrat.

Not to forget I want to thank the teams of ADIC and YRLS. It was a pleasure working with you and I hope that you keep up the important support of students at Curie and world wide.

I also want to thank my dear friend Stefan Thielen for his help and support regardless of the hundreds and thousands of kilometers separating us. Live long and prosper!

Although coming at the end, they are playing the most important role in my life. I want to thank my family for their support no matter what. For the motivational debates, and consulting in any situation of life.

Last but not least I want to thank my beloved wife, who supported me throughout the last eight years. Always standing by my side at any thinkable situation "for better, for worse, for richer, for poorer, in sickness and in health".

Erklärung:

Ich versichere, dass ich diese Arbeit selbstständig verfasst und keine anderen als die angegebenen Quellen und Hilfsmittel benutzt habe.

Heidelberg, den 07. November 2016 .....

Unterschrift